Fall 11-2011

SIMULATION AND FABRICATION OF 3D SPIRAL PHOTONIC CRYSTALS AS CIRCULAR POLARIZERS

Xuejian Li
University of Nebraska – Lincoln, hustlxj@gmail.com

SIMULATION AND FABRICATION OF 3D SPIRAL PHOTONIC CRYSTALS AS CIRCULAR POLARIZERS

by

Xuejian Li

A THESIS

Presented to the Faculty of

The Graduate College at the University of Nebraska

In Partial Fulfillment of Requirements

For the Degree of Master of Science

Major: Electrical Engineering

Under the Supervision of Professor Natale J. Ianno

Lincoln, Nebraska

November, 2011

SIMULATION AND FABRICATION OF 3D SPIRAL PHOTONIC CRYSTALS AS CIRCULAR POLARIZERS

Xuejian Li, M.S.
University of Nebraska, 2011
Advisor: Natale J. Ianno

Three-dimensional (3D) spiral photonic crystals (PhCs) have a periodic varied refractive index (RI) with the periodicity comparable to the wavelength of incident light. They can pass circularly polarized (CP) light with handedness opposite to their own structures' handedness while block the polarization state with the same handedness. Three-dimensional spiral PhCs for use as circular polarizers have two main advantages over conventional circular polarizers. On the one hand, it has wide operation wavelength based on the photonic band gap caused by PhCs and the interaction between CP light and each individual spiral structure. On the other hand, the height of each spiral structure can be made within the range of several incident light's wavelengths, therefore, compact circular polarizers can be fabricated through 3D spiral PhCs.

In this work, the Finite-difference time domain (FDTD) method was used to investigate the circular polarization selection of 3D spiral PhCs. Optical transmittance spectra of 3D spiral PhCs illuminated by two orthogonal CP lights have been calculated. Transparent materials with different RIs were adapted to demonstrate that higher RI material could have broader operation wavelength. Furthermore, dispersive materials like aluminum with different structures and pitch numbers were investigated to increase the operation wavelength of 3D spiral PhCs.

Fabrication work was aimed at high-quality 3D spiral PhCs with operation in the near-infrared range. The FDTD tool was utilized to predict the transmittance of 3D spiral PhCs based on transparent and dispersive materials.

Three-dimensional spiral PhCs were fabricated from glassy arsenic trisulfide (As_2S_3) with high RI (n=2.45). This material was chosen to strongly modulate the light propagation and to obtain a broader operation band. Thermal vapor deposition was used to prepare the desired thickness of As_2S_3 thin films as photoresists. A laser direct writing system based on two-photon absorption was used to achieve 3D micro-structure fabrication by point-by-point laser exposure. The unexposed area was removed with appropriate development solution to reveal the 3D spiral PhCs. Large size (280 μm by 280 μm) spiral PhCs were fabricated.

Acknowledgements

I would first like to thank my advisor, Professor Ianno Natale. He treats students like peers. I am always very comfortable when asking him any equations. No matter what academic problems I may have, he will stop what he is currently working on and discuss with me about my project or we will go together to the laboratory. His honest, caring and easy-going personality also inspires me a lot.

Second, I also would like to express my sincere thanks to my committee members, Professor Yongfeng Lu and Professor Schubert Mathias. During my master program, they gave adequate help and support for my academic work.

Thirdly, I would like to thank Dr. Hao Wang, Wei Xiong, Weiqing Yang and other postdoc and graduate students from Dr. Ianno's, Dr. Lu's and Dr. Schubert's group. They not only give me support on my academic side but also have made my life in Lincoln easier and more colorful.

Last but not least, my thanks to my parents, my fiancé and my younger sister. They give me unlimited courage in my dark time and share my happy moment all the time. I love you all.

TABLE OF CONTENTS

LIST OF FIGURES

CHAPTER 1 INTRODUCTION

1.1 Motivations

A circular polarizer is a device that distinguishes between different circularly polarized (CP) light based on the polarization states in a specific wavelength range. It has many applications in optical communications, optical remote sensors, color displays [1, 2] and circular dichroism imaging microscopy [3]. A conventional circular polarizer is a combination of a quarter wave plate and a linear polarizer. In the past ten years, researchers found chiral planar metamaterials exhibit circular polarization selection effect [4]. In the same year 2007, 3D spiral photonic crystals [5] were fabricated and designed to demonstrate that these could have much higher distinction ratio (optical transmittance contrast between two polarization states) than planar chiral metamaterials. Three dimensional spiral PhCs are a subclass of photonic crystals. They exhibit a photonic band gap (PBG) like other PhCs and additionally process unique polarization selection effect – they can only pass left- or right- handed circularly polarized light based on their own structure handednesses. Three dimensional spiral PhCs as circular polarizers surpass conventional circular polarizers because they can be made more compact and also have broader operation wavelength.

Photonic crystals have periodically alternating high and low refractive indices which can confine and guide the light propagation [6, 7]. Photonic crystals with PBG are comparable to semiconductors which form an electronic bang gap. Based on their high photon localization and low-loss transmission, photonic crystals have been rapidly developed for super-lens [8], waveguide [9], light-emitting diode [10] and photonic crystal fibers [11]. At first, the structures of PhCs were generally restricted to few structures like the woodpile-shape [12] and the layer-by-layer particle thin film [13].

With the maturity of laser direct writing (LDW) based on two-photon absorption [14],3D spiral PhCs can be fabricated as an important class in the PhC family.

Laser direct writing is a very powerful tool for the fabrication of arbitrary microstructures. Based on two-photon absorption, photoresist will only be exposed in the focal point. Therefore, while conventional lithography can only manufacture a 2D pattern, 3D microstructures can be obtained by the LDW system. By using laser direct writing, researchers have obtained “slanted pore” [12], woodpile [15] , and spiral [16] PhCs.

In this work, the polarization selection property of 3D spiral PhCs with the help of the finite-difference time domain (FDTD) method has been demonstrated. Optical transmittances of transparent and dispersive materials were calculated by using the FDTD method. Simulation results showed 3D spiral PhCs based on As_2S_3 with higher refractive index (RI) or more pitch numbers had broader operation wavelength than low RI materials. For the dispersive materials, increased pitch numbers of spiral structures present more obvious polarization selection effect while double-helix spiral structures have broader operation wavelength then the single-helix spiral structures.

Three dimensional spiral PhCs with lattice constants in the near infrared spectra were fabricated by LDW. The writing parameters including laser power, defocus factor and structure size as well as etching time and the concentration of the development solution were optimized. Glassy arsenic trisulfide (As_2S_3) was used as a photoresist because of its high RI (n=2.45) and strong mechanical support. In contrast, traditional photoresist’s RI was relatively low (n=1.5) with instability under high temperature environment and poor mechanical strength.

1.2 Thesis Outline

Chapter 2 will briefly introduce the basics of polarization optics, interactions between circularly polarized light with spiral PhCs and the basic theory of PhCs. In Chapter 3, transparent and dispersive materials will be used for transmittance calculation. The polarization selection property of 3D spiral PhCs based on different RIs and pitch numbers of 3D spiral structures will be investigated. The fabrication part in Chapter 4 will focus on the photoresist preparation by thermal vapor deposition, 3D spiral PhCs writing by laser direct writing system and the photoresist development. Two-photon absorption will be discussed to demonstrate the mechanism of 3D microstructure fabrication. Many writing and development parameters like laser power defocus factor, structure size, etching time and the development solution concentration are optimized to improve the quality of the 3D spiral PhCs. Scanning electron microscopy graphs are obtained to prove the good quality of 3D spiral PhCs. In Chapter 5, our current achievements and proposed future work are summarized.

References

1. Yoshioka, T., et al., *Reversible-photon-mode full-color display by means of photochemical modulation of a helically cholesteric structure.* Advanced Materials, 2005. **17** (10): p. 1226-1229.

2. De Filpo, G., F.P. Nicoletta, and G. Chidichimo, *Cholesteric emulsions for colored displays.* Advanced Materials, 2005. **17** (9): p. 1150-1152.

3. Claborn, K., et al., *Circular dichroism imaging microscopy: Application to enantiomorphous twinning in biaxial crystals of 1,8-dihydroxyanthraquinone.* Journal of the American Chemical Society, 2003. **125** (48): p. 14825-14831.

4. Decker, M., et al., *Circular dichroism of planar chiral magnetic metamaterials.* Optics Letters, 2007. **32** (7): p. 856-858.

5. Thiel, M., et al., *Polarization stop bands in chiral polymeric three-dimensional photonic crystals.* Advanced Materials, 2007. **19** (2): p. 207-210.

6. Yablonovitch, E., *Inhibited Spontaneous Emission in Solid-State Physics and Electronics.* Physical Review Letters, 1987. **58** (20): p. 2059.

7. John, S., *Strong localization of photons in certain disordered dielectric superlattices.* Physical Review Letters, 1987. **58** (23): p. 2486.

8. Foteinopoulou, S. and C.M. Soukoulis, *Negative refraction and left-handed behavior in two-dimensional photonic crystals.* Physical Review B, 2003. **67**.

9. Mekis, A., et al., *High Transmission through Sharp Bends in Photonic Crystal Waveguides.* Physical Review Letters, 1996. **77** (18): p. 3787.

10. Byeon, K.-J., S.-Y. Hwang, and H. Lee, *Fabrication of two-dimensional photonic crystal patterns on GaN-based light-emitting diodes using thermally curable monomer-based nanoimprint lithography.* Applied Physics Letters, 2007. **91** (9).

11. Russell, P., *Photonic crystal fibers.* Science, 2003. **299** (5605): p. 358-362.

12. Lin, S.Y., et al., *A three-dimensional photonic crystal operating at infrared wavelengths.* Nature, 1998. **394** (6690): p. 251-253.

13. Ozin, G.A. and S.M. Yang, *The race for the photonic chip: Colloidal crystal assembly in silicon wafers.* Advanced Functional Materials, 2001. **11** (2): p. 95-104.

14. Gansel, J.K., et al., *Gold Helix Photonic Metamaterial as Broadband Circular Polarizer.* Science, 2009. **325** (5947): p. 1513-1515.

15. Deubel, M., et al., *Direct laser writing and characterization of "Slanted Pore" Photonic Crystals.* Applied Physics Letters, 2004. **85** (11): p. 1895-1897.

16. Staude, I., et al., *Fabrication and characterization of silicon woodpile photonic crystals with a complete bandgap at telecom wavelengths.* Optics Letters, 2010. **35** (7): p. 1094-1096.

CHAPTER 2 BACKGROUND

Photonic crystals without chirality couldn't distinguish the circularly polarized (CP) light with different polarization states. Three dimensional spiral PhCs can not only perform like common PhCs with PBGs but also distinguish CP light with different handednesses. In order to understand the polarization states of light and the basic theories of 3D spiral PhCs, section 2.1 introduces the mathematic expression of polarized light and the interaction between light and materials. Section 2.2 presents the definition and optical properties of PhCs derived from Maxwell equations and the unique advantages of direct laser writing (DLW) system compared with other methods for 3D PhCs fabrication.

2.1 Polarization optics

2.1.1 Mathematic expression of polarized light

Polarized light can be represented as the vector sum of two orthogonal electric fields [1].

$$\vec{E} = \vec{E}_x(z,t) + \vec{E}_y(z,t) \tag{2.1}$$

$$\vec{E}_x(z,t) = \hat{x} E_{0x} \cos(kz - wt) \tag{2.2}$$

$$\vec{E}_y(z,t) = \hat{y} E_{0y} \cos(kz - wt + \theta) \tag{2.3}$$

where θ is the relative phase difference between the two orthogonal waves, both of which are traveling along the z direction. From Eqs (2.1) to (2.3), we can easily find that $\vec{E}$ is rotating along z direction upon propagation. The endpoint of $\vec{E}$ will trace out an ellipse. By removing the $(kz - wt)$ dependence, Eqs (2.1) to (2.3) lead to:

$$\left(\frac{E_y}{E_{0y}}\right)^2 + \left(\frac{E_x}{E_{0x}}\right)^2 - 2\left(\frac{E_x}{E_{0x}}\right)\left(\frac{E_y}{E_{0y}}\right)\cos(\theta) = \sin^2(\theta) \tag{2.4}$$

FIGURE 2.1shows three polarization configurations when $E_{0x} = E_{0y}$. For CP light, two requirements $\theta = \pm \pi/2$ and $E_{0x} = E_{0y}$ are needed. The tip of $\vec{E}$ will trace a helix. When we look at the series of tips by following the propagation axis, the endpoints form a circle. If $\theta = -\pi/2$, the polarization is called right circular polarization (RCP) light; while $\theta = +\pi/2$, it is left circular polarization light (LCP). The linear polarization will be formed when $\varepsilon = 0$ or $\pm\pi$. Generally speaking, if $E_{0x} = E_{0y}$, varied phase difference θ yields various polarization configurations.

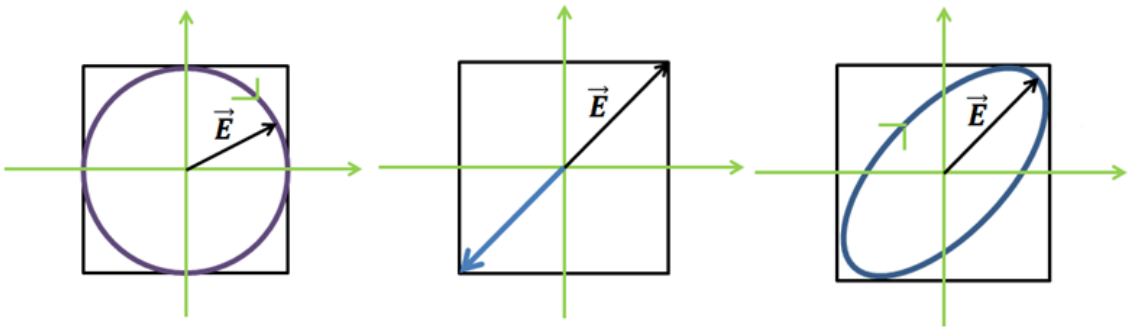

FIGURE 2.1 Various polarization configurations: (a) circular, (b) linear, (c) elliptical polarization.

2.1.2 Interaction between light and materials

Polarization selection refers to the selective absorption of one of two orthogonal electric fields. For the circular polarization selection of circular polarizers, they have preferred absorption on LCP or RCP while passing RCP or LCP.

Conventional circular polarizers consist of a quarter wave plate and a linear polarizer. A quarter wave plate is an optical element that introduces a phase relative shift of $\theta = \pi/2$. By introducing the $\pi/2$ phase change, it can convert LCP and RCP light into orthogonal

polarized (LP) light. With one LP light parallel to the principle axis of linear polarizer, this LP light can pass the linear polarizer while another LP light perpendicular to the principle axis. FIGURE 2.2 shows the optical configuration of conventional circular polarizers.

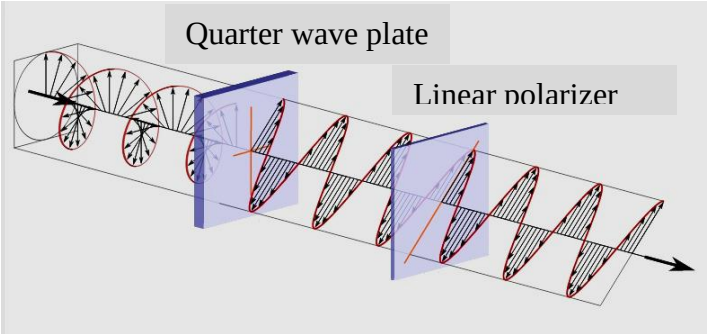

FIGURE 2.2 Optical configuration of conventional circular polarizers[2].

Three dimensional spiral PhCs use a different mechanism than conventional circular polarizers to achieve the polarization selection. The polarization selection mechanism is based on the interference within the structure which results in total reflection for one polarization state but large transmittance for another polarization state. If we slice the spiral structure into many layers, the spiral structure is working exactly like cholesteric liquid crystal structure as shown in FIGURE 2.3. When the pitch is of the same order as the wavelength, this can cause cholesteric liquid crystal structure to exhibit Bragg reflection to the circularly polarized light having the same handedness with the structure. The center wavelength $\lambda_0 = \mathrm{p} * \mathrm{n}$ while the operation bandwidth $\Delta\lambda = \mathrm{p} * \Delta\mathrm{n}$, where $\Delta\mathrm{n}$ is the refractive index contrast in parallel and perpendicular direction.

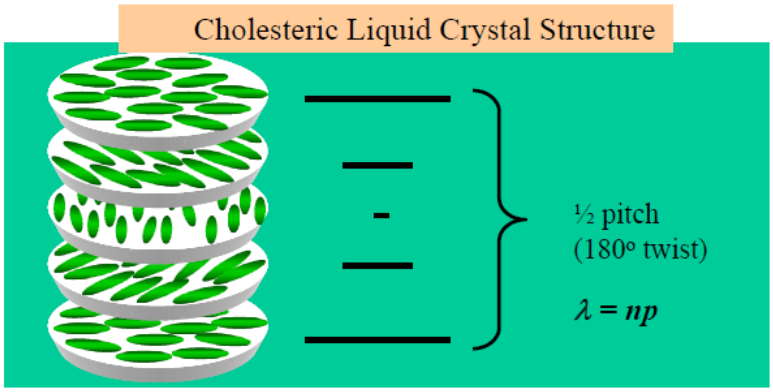

FIGURE 2.3 Cholesteric liquid crystal structure; p and n refers to the chiral pitch and refractive index respectively [3].

2.2 Photonic crystals

2.2.1 Definition of photonic crystals

Photonic crystals have periodic variation in refractive index. They can be classified by one-, two- and three-dimensional photonic crystals as shown in FIGURE 2.4 [5]. Photonic crystals with varied refractive index in one, two or three direction(s) are respectively called one- two- and three-dimensional photonic crystals.

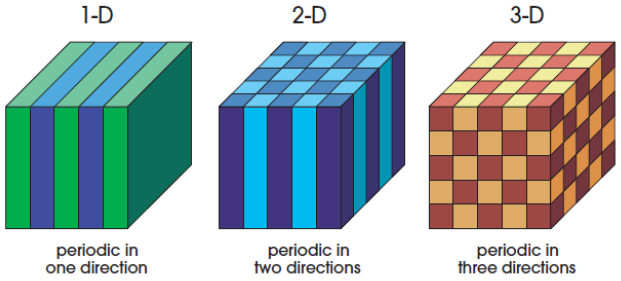

FIGURE 2.4 Examples of one-, two- and three-dimensional photonic crystals. The different colors in the graphs stands for different refractive indices. [4]

A quarter-wave stack is a widely used optical device which consists of alternate layers with different RIs. Incident light with proper wavelength can be fully reflected because of the interference effects among multiple light beams reflected from each interface. In

FIGURE 2.5, the diffraction relationship with wave vector vs frequency is plotted with different dielectric constant contrast. With larger dielectric constant contrast, wide PBG can be formed [5].

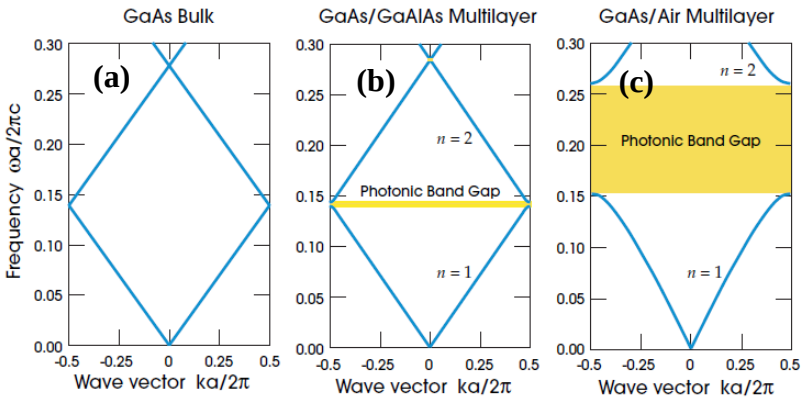

FIGURE 2.5 The diffraction relationship between wave vector and frequency. (a): dielectric constant contrast $\varepsilon_1 : \varepsilon_2 = 13:13$. (b): $\varepsilon_1 : \varepsilon_2 = 13:12$. (c): $\varepsilon_1 : \varepsilon_2 = 13:1$. [4]

Compared with one-dimensional photonic crystals, two-dimensional crystals can confine light propagation in two directions. Wave guides based on two-dimensional photonic crystals have been made [6]. More interestingly, three-dimensional PhCs can modulate light propagation in all three directions [7].

2.2.2 Eigenmodes of photonic crystals

Eigenmodes are the certain frequencies of the light that can exist in photonic crystals. Maxwell's equations are a good starting point for understanding photonic crystals. In SI units, these four equations are:

$$\nabla \bullet \vec{B} = 0 \tag{2.5 a}$$

$$\nabla \times \vec{E} + \frac{\partial \vec{B}}{\partial t} = 0 \tag{2.5 b}$$

$$\nabla \bullet \vec{D} = \rho \tag{2.5 c}$$

$$\nabla \times \vec{H} - \frac{\partial \vec{D}}{\partial t} = \vec{J} \qquad (2.5\ d)$$

The PhCs usually don't vary with time, and they don't carry free charges or currents. Therefore, we can set $\rho = 0$ and $\vec{J} = 0$. Furthermore, some assumptions are considered for simplifying these above equations. Firstly, in most cases, the field strengths are very small. Under this case, the electric field $\vec{E}$ and electrical displacement field $\vec{D}$ is linear. Secondly, the material is assumed to be isotropic and non-dispersive. Therefore, $\vec{\varepsilon}_r$ is scalar and independent of light frequencies. Thirdly, for most dielectric materials, the relative magnetic permeability μ varies only slightly. Therefore, this term can be ignored. Combining all above assumptions [5], Maxwell's equations can be simplified to

$$\nabla \bullet \vec{H}(\vec{r}, t) = 0 \qquad (2.6\ a)$$

$$\nabla \times \vec{E}(\vec{r}, t) + \mu_0 \frac{\partial \vec{H}(r, t)}{\partial t} = 0 \qquad (2.6\ b)$$

$$\nabla \bullet [\varepsilon(\vec{r})\vec{E}(\vec{r}, t)] = 0 \qquad (2.6\ c)$$

$$\nabla \times \vec{H}(\vec{r}, t) - \varepsilon_0 \varepsilon(\vec{r}) \frac{\partial \vec{E}(\vec{r}, t)}{\partial t}] = 0 \qquad (2.6\ d)$$

Both $\vec{E}$ and $\vec{H}$ vary sinusoidally (harmonically) with time. Therefore, we can write a harmonic mode as the following format:

$$\vec{H}(\vec{r}, t) = \vec{H}(\vec{r}) e^{-i\omega t} \qquad (2.7\ a)$$

$$\vec{E}(\vec{r}, t) = \vec{E}(\vec{r}) e^{-i\omega t} \qquad (2.7\ b)$$

Substituting Eqs. (2.6) and (2.7), we can eliminate time dependence to get the following equations:

$$\nabla \bullet \vec{H}(\vec{r}) = 0 \tag{2.8 a}$$

$$\nabla \times \vec{E}(\vec{r}) + i\omega\mu_0 \frac{\partial \vec{H}(r)}{\partial t} = 0 \tag{2.8 b}$$

$$\nabla \bullet [\varepsilon(\vec{r})\vec{E}(\vec{r})] = 0 \tag{2.8 c}$$

$$\nabla \times \vec{H}(\vec{r}) + i\omega\varepsilon_0\varepsilon(\vec{r})\frac{\partial \vec{E}(\vec{r})}{\partial t}] = 0 \tag{2.8 d}$$

Solving Eqs. 2.8(b) and 2.8(d) together, we finally get the master equation

$$\nabla \times \left(\frac{1}{\varepsilon(\vec{r})} \nabla \times \vec{H}(\vec{r}) \right) = \left(\frac{\omega}{c} \right)^2 \vec{H}(\vec{r}) \tag{2.9}$$

By using Eqs 2.7(a) and 2.7(c) and the master equation together, we can determine $\vec{H}(\vec{r})$.

Using Eqs 2.8(b) and 2.8(d), we can derive $\vec{E}(\vec{r})$ mode from $\vec{H}(\vec{r})$.

Eigenmodes of 3D spiral PhCs

The polarization stop band can be predicted by solving the master equation to get the eigenmodes. By using the plane-wave expansion method, Chan has theoretically demonstrated 3D spiral PhCs can only allow one of the orthogonal circular polarizations [5]. The schematic diagram of the spiral structure and its Brillouin points is shown in FIGURE 2.6.

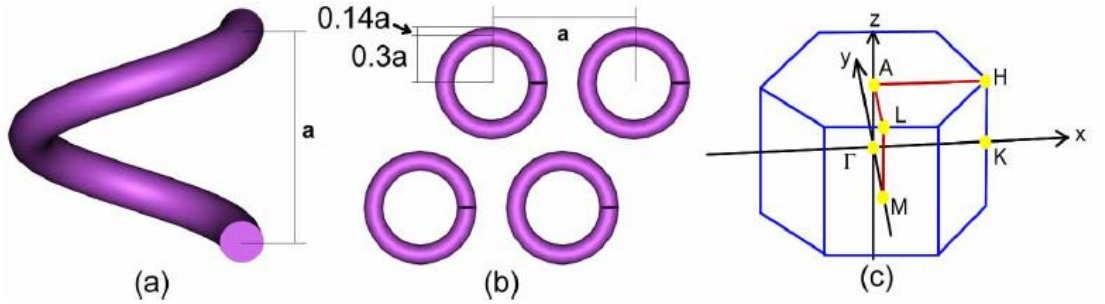

FIGURE 2.6 A schematic diagram of the spiral structure and its Brillouin points. (a) and (b) are size view and top view of the spiral structures respectively. (c) is the Brillouin zone of spiral structures with triangular symmetry. [7]

The transmission spectra and the band structure of the right-handed (RH) spiral structure are shown in FIGURE 2.7. The yellow bar in FIGURE 2.7 (c) clearly showed that there is a polarization gap in the second band.

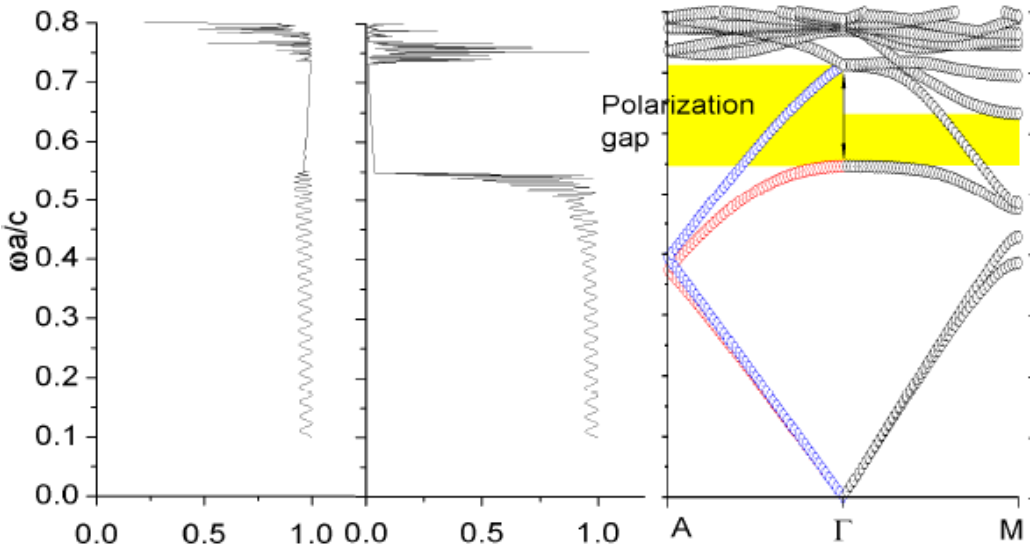

FIGURE 2.7 Transmission spectra and the band structure of RH spiral structure shown in Fig. (2.6). (a) and (b) are the transmittance of the LH and RH polarizations respectively. The dispersion relationship is shown in (c). The first and second bands of the two orthogonal polarizations are marked with red and blue colors respectively [7].

2.2.3 Basic properties of photonic crystals

Based on light confinement and localization of PhCs, many promising applications have been achieved. For example, 3D PhCs can guide light propagation with very low energy loss. Also, a narrow band filter can be made by selectively passing the desired frequencies. For homogeneous medium, the speed of light is inversely proportional to the RI of the medium as described by Eq. (2.10). For PhCs as non-homogenous medium, there is a PBG between top and bottom band as shown in FIGURE 2.5 (c). All properties of PhCs result from their PBG.

$$\omega(k) = \frac{ck}{\sqrt{\varepsilon}} \tag{2.10}$$

Photonic bang gap

According to electromagnetic energy and the vibrational principle [4], the high frequency modes have a larger proportion of their energy in low $-\varepsilon$ regions while the low frequency modes mainly concentrate in the high $-\varepsilon$ regions as shown in FIGURE 2.5.

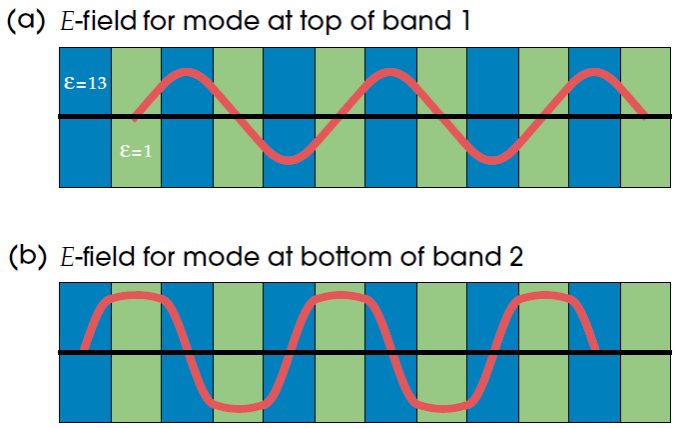

FIGURE 2.8 The modes associated with the lowest band gaps shown in Figure 2.5(c). The RI ratio is 13:1.

Based on the energy redistribution in high and low refractive index materials, PBGs are formed. The width of the band gap is proportional to the dielectric contrast ($\Delta\varepsilon = \varepsilon_2 - \varepsilon_1$).

Over the years, high RI 3D photonic crystals with larger band gaps have been fabricated by various methods like repetitive deposition and etching of multiple dielectric films [8] and silicon chemical vapor deposition (CVD) [9].

Scalability

Scalability is a unique feature of electromagnetism in dielectric material. It means that we can determine all other length scales from the solution at one wavelength scale. In the far-field situation, Maxwell equations of PhCs are scalable. Therefore, its solutions are scalable. This conclusion has been drawn in reference 7 through a relatively simple scale transformation. The scaling property is very useful for fabrication process. For example, larger scales of PhCs can be fabricated to predict the optical performances of smaller scales when the smaller scales are difficult to fabricate under current experimental circumstances.

We need to note that when the dielectric constant is dependent on the size [10], the scaling law won't be applicable anymore. Furthermore, most of the dielectric materials are dispersive which make the scalability of the PhCs not applicable. However, if the dielectric materials are not highly dispersive, scalability is still a good approximation tool.

Time reversal symmetry

Time reversal symmetry is another important property of the PhCs. It means that Eq. (2.9) is invariant when we change the sign of the time variable. The dispersion relation has inversion symmetry based on the time reversal symmetry [7]. Eq. (2.10) shows the inversion symmetry of the dispersion relation.

$$\omega_{-\vec{kn}} = \omega_{\vec{kn}} \tag{2.10}$$

Eq. (2.10) is still applicable even if the PhCs don't exhibit inversion symmetry.

2.2.4 Fabrication of PhCs

Extensive investigations of the fabrication of PhCs can be found in some review articles [11, 12]. One dimensional PhCs have been produced and used for a long time. It has wide application in anti-reflection coating, notch filters and distributed Bragg reflectors. All of them are essentially a stack of films. However, the fabrication of 2D and 3D PhCs are challenging. Since two seminal papers published in 1987 [13, 14] to theoretically prove 3D PhCs can guide and confine light propagation with minimum energy loss, researchers from all around the world have proposed various methods to fabricate PhCs. The first 3D PhCs with complete PBG [15] were fabricated by drilling millimeter holes with chemical-beam-assisted ion etching. The size leads to its operation wavelength to be in the microwave regime. Based on whether the 3D PhCs are fabricated by building up basic units or from bulk materials, all fabrication methods can be categorized into two kinds of methods: "bottom-up" or "top-down" approaches.

Self-assembly is a common bottom-up growth method with the usage of colloidal crystals [16]. Colloids refer to the structures comprising small particles suspended in a liquid. By immersing substrate into colloidal crystals, particles will be deposited in a periodic array on the surface of substrate layer-by-layer after removing the solvent under the temperature near the boiling point [17-19]. Usually, the colloidal crystals will be infiltrated with various materials for increasing RI contrast or implanting functions from other materials like silicon [20,21], stibnite (Sb_2S_3) [22], Indium phosphide (InP) [23]

and titania (TiO_2) [24]. Self-assembly is very suitable for low-cost and large area 3D photonic crystals [25]. However, it has two disadvantages. On the one hand, because of the defects, the long-range highly organized 3D PhCs are difficult to fabricate. Therefore, the 3D PhCs sample obtained by self-assembly is not strictly true 3D PhCs because its structure is not completely periodic. On the other hand, only certain structures such as face-centered cubic structure can be fabricated (FCC) [26,28].

Glancing angle deposition (GLAD) is another popular bottom-up method to produce photonic crystals. During the GLAD process, the vapor flux arrives at the substrate with an oblique angle from the substrate normal. The resulting structures grow towards the vapor source. Therefore, with substrate rotation, spiral structures can be made [29, 30].

Based on multiple-beam interference, holographic lithography is widely used to fabricate 2D and 3D PhCs [31-34]. It's a top-down fabrication method. Because the light intensity distribution is periodic through optical light interference, photo-resist is periodically exposed. After the development procedure, the exposed area can be kept or removed depending on whether photo-resist is negative or positive. Large-scale (over 1 cm^2) high-quality 3D FCC-type PhCs structures can be produced by using a simple single refracting prism holographic lithography technique [35]. However, like self-assembly methods, holographic lithography is restricted to fabricating limited structures such as the simple cubic, diamond-like, gyroid-like[32] and FCC structure [31, 33].

The LDW approach is an innovative and promising top-down method which has true 3D fabrication capability. In the LDW system, femtosecond laser pulses are tightly focused in the photoresist when the laser intensity is below to the two-photon absorption threshold. In contrast, at the focal point, the laser intensity is above the two-photon

threshold. Due to two-photon absorption, the photoresist will be exposed. By moving the relative position between the sample stage and laser focal point, the desired places can be exposed by femtosecond pulses. In negative photoresist, the exposed area will be revealed; the exposed area will be removed for the positive photoresist. Three dimensional nanostructures with feature size smaller than 100nm [36-39] have been fabricated by overcoming the diffraction limit. The minimum feature size down to 40nm has been achieved in 2009 by one-color initiation and deactivation of polymerization [39]. Among all fabrication mentioned above, laser direct writing is the only method having the capability to arbitrarily fabricate various structures such as spirals [40, 41], woodpile structures [42,43] , “slanted pore” structures [44] and quasicrystals [45,46]. Furthermore, the fabricated structures used as templates and infiltrated with gold [47], silicon [42, 43] or other semiconductor and metals for optical performance modifications.

FIGURE 2.9 shows 3D PhCs fabricated by different approaches.

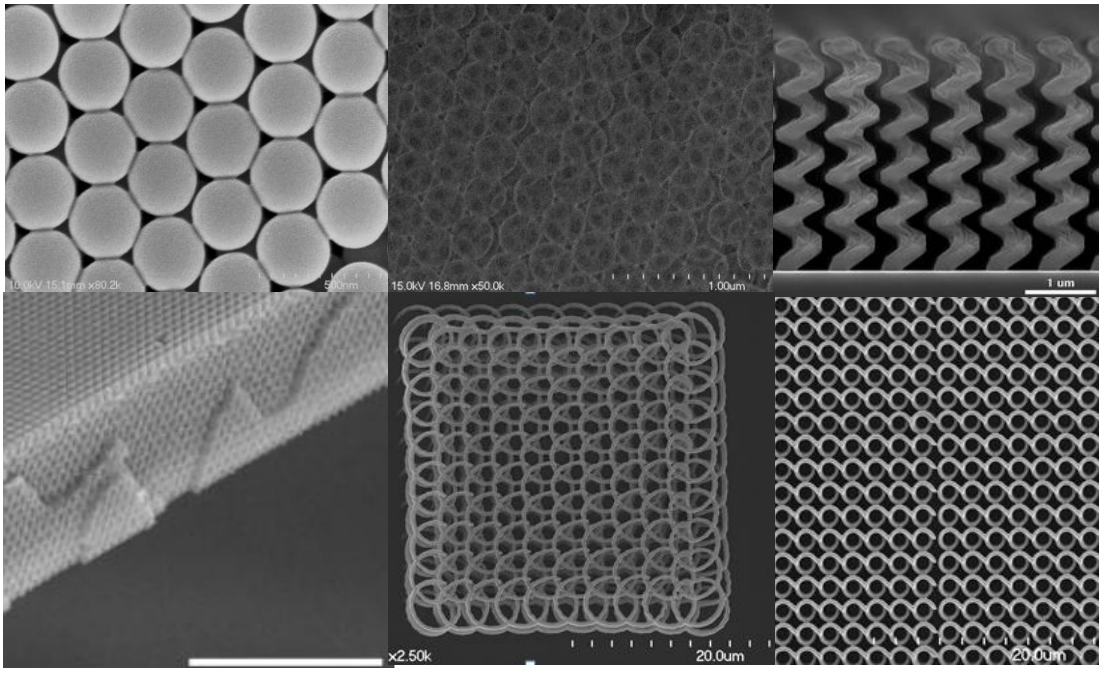

FIGURE 2.9 3D PhCs fabricated by (a) self-assembly of colloidal (b) self-assembly plus CVD deposition and hydrofluoric acid etching, (c) glancing angle deposition [46], (d) holographic lithography [29], scar bar: 10 μm, (e-f) LDW system based on IP-L and $As_2 S_3$ chalcogenide glass.

References

1. Hecht, E., *Optics,* 4th edition, 2001

2. http://en.wikipedia.org/wiki/Polarizer, 2011

3. http://www.chelix.com/pdfs/HPP_pigment_overview.pdf, 2011

4. Kraus, J. D. and R. J. Marhefka, *Antennas: for All Applications,* 3rd ed. 2003: McGraw-Hill.

5. Joannopoulos. J.D., et al.,, *Photonic Crystals:Molding the Flow of Light,* 2nd ed. 2008: Princeton University Press.

6. Mekis, A., et al., *High Transmission through Sharp Bends in Photonic Crystal Waveguides.* Physical Review Letters, 1996. **77**(18): p. 3787.

7. Lee, J.C.W. and C.T. Chan, *Polarization gaps in spiral photonic crystals.* Optics Express, 2005. **13**(20): p. 8083-8088.

8. Lin, S.Y., et al., *A three-dimensional photonic crystal operating at infrared wavelengths.* Nature, 1998. **394**(6690): p. 251-253.

9. Wang, H. and Y.F. Lu, *Core-shell photonic band gap structures fabricated using laser-assisted chemical vapor deposition.* Journal of Applied Physics, 2008. **103**(1).

10. Qu, B.D., et al., *Size and temperature-dependence of dielectric-constant of ultrafine pbtio3 particles.* Chinese Physics Letters, 1994. **11**(8): p. 514-517.

11. Sakoda, K., “Optical Properties of Photonic Crystals," Springer-Verlag (2001).

12. Lopez, C., *Materials aspects of photonic crystals.* Advanced Materials, 2003. **15**(20): p. 1679-1704.

13. Krauss, T.F. and R.M. De la Rue, *Photonic crystals in the optical regime - past, present and future.* Progress in Quantum Electronics, 1999. **23**(2): p. 51-96.

14. Yablonovitch, E., *Inhibited Spontaneous Emission in Solid-State Physics and Electronics.* Physical Review Letters, 1987. **58**(20): p. 2059.

15. John, S., *Strong localization of photons in certain disordered dielectric superlattices.* Physical Review Letters, 1987. **58**(23): p. 2486.

16. Yablonovitch, E., T.J. Gmitter, and K.M. Leung, *Photonic band structure: The face-centered-cubic case employing nonspherical atoms.* Physical Review Letters, 1991. **67**(17): p. 2295-2298.

17. Xia, Y.N., et al., *Monodispersed colloidal spheres: Old materials with new applications.* Advanced Materials, 2000. **12**(10): p. 693-713.

18. Xia, Y.N., Gates, B. and Li, Z.Y., *Self-assembly approaches to three-dimensional photonic crystals.* Advanced Materials, 2001. **13**(6): p. 409-413.

19. Norris, D.J., et al., *Opaline photonic crystals: How does self-assembly work?* Advanced Materials, 2004. **16**(16): p. 1393-1399.

20. S.H. Im,, et al., *Three-dimensional self-assembly of colloids at a water-air interface: A novel technique for the fabrication of photonic bandgap crystals.* Advanced Materials, 2002. **14**(19): p. 1367-1369.

21. Hermatschweiler, M., et al., *Fabrication of silicon inverse woodpile photonic crystals.* Advanced Functional Materials, 2007. **17**(14): p. 2273-2277.

22. Tetreault, N., Miguez, H. and Ozin, G.A., *Silicon inverse opal - A platform for photonic bandgap research.* Advanced Materials, 2004. **16**(16): p. 1471-1476.

23. Juarez, B.H., et al., *High-energy photonic bandgap in Sb2S3 inverse opals by sulfidation processing (vol 15, pg 319, 2003).* Advanced Materials, 2003. **15**(6): p. 478-478.

24. H.M. Yates,, et al., *Modification of the natural photonic bandgap of synthetic opals via infilling with crystalline InP.* Advanced Functional Materials, 2005. **15**(3): p. 411-417.

25. Zhu, Y., et al., *Three-dimensional photonic bandgap crystals of titania hollow spheres at visible wavelengths.* Applied Physics a-Materials Science & Processing, 2009. **94**(4): p. 731-734.

26. Ozin, G.A. and S.M. Yang, *The race for the photonic chip: Colloidal crystal assembly in silicon wafers.* Advanced Functional Materials, 2001. **11**(2): p. 95-104.

27. Ding, J., Chen, D. and Tang, F.Q., *Fabrication of photonic band gap crystals through colloid self-assembly methods.* Progress in Chemistry, 2004. **16**(4): p. 492-499.

28. Landon, P.B. and Glosser, R., *Self-assembly of spherical colloidal silica along the 100 direction of the FCC lattice and geometric control of crystallite formation.* Journal of Colloid and Interface Science, 2004. **276**(1): p. 92-96.

29. Summers, M.A., et al., *Fabrication of 2D-3D photonic crystal heterostructures by glancing angle deposition.* Photonics and Nanostructures-Fundamentals and Applications, 2009. **7**(2): p. 76-84.

30. Summers, M.A. and Brett, M.J., *Optimization of periodic column growth in glancing angle deposition for photonic crystal fabrication.* Nanotechnology, 2008. **19**(41).

31. Campbell, M., et al., *Fabrication of photonic crystals for the visible spectrum by holographic lithography.* Nature, 2000. **404**(6773): p. 53-56.

32. Ullal, C.K., et al., *Photonic crystals through holographic lithography: Simple cubic, diamond-like, and gyroid-like structures.* Applied Physics Letters, 2004. **84**(26): p. 5434-5436.

33. Xu, D., et al., *Phase tunable holographic fabrication for three-dimensional photonic crystal templates by using a single optical element.* Applied Physics Letters, 2009. **94**(23).

34. Wang, X., et al., *Three-dimensional photonic crystals fabricated by visible light holographic lithography.* Applied Physics Letters, 2003. **82**(14): p. 2212-2214.

35. Wu, L.J., et al., *Fabrication of large area two- and three-dimensional polymer photonic crystals using single refracting prism holographic lithography.* Applied Physics Letters, 2005. **86**(24).

36. Maruo, S., O. Nakamura, and S. Kawata, *Three-dimensional microfabrication with two-photon-absorbed photopolymerization.* Optics Letters, 1997. **22**(2): p. 132-134.

37. LaFratta, C.N., et al., *Multiphoton fabrication.* Angewandte Chemie-International Edition, 2007. **46**(33): p. 6238-6258.

38. Maruo, S. and J.T. Fourkas, *Recent progress in multiphoton microfabrication.* Laser & Photonics Reviews, 2008. **2**(1-2): p. 100-111.

39. Li, L.J., et al., *Achieving lambda/20 Resolution by One-Color Initiation and Deactivation of Polymerization.* Science, 2009. **324**(5929): p. 910-913.

40. Seet, K.K., et al., *Three-dimensional horizontal circular spiral photonic crystals with stop gaps below 1 mu m.* Applied Physics Letters, 2006. **88**(22).

41. Seet, K.K., et al., *Three-dimensional spiral-architecture photonic crystals obtained by direct laser writing.* Advanced Materials, 2005. **17**(5): p. 541-545.

42. Hermatschweiler, M., et al., *Fabrication of silicon inverse woodpile photonic crystals.* Advanced Functional Materials, 2007. **17**(14): p. 2273-2277.

43. Tetreault, N., et al., *New route to three-dimensional photonic bandgap materials: Silicon double inversion of polymer templates.* Advanced Materials, 2006. **18**(4): p. 457-460.

44. Deubel, M., et al., *Direct laser writing and characterization of "Slanted Pore" Photonic Crystals.* Applied Physics Letters, 2004. **85**(11): p. 1895-1897.

45. Ledermann, A., et al., *Three-dimensional silicon inverse photonic quasicrystals for infrared wavelengths.* Nature Materials, 2006. **5**(12): p. 942-945.

46. Ledermann, A., M. Wegener, and G. von Freymann, *Rhombicuboctahedral Three-Dimensional Photonic Quasicrystals.* Advanced Materials, 2010. **22**(21): p. 2363-2366.

47. Gansel, J.K., et al., *Gold Helix Photonic Metamaterial as Broadband Circular Polarizer.* Science, 2009. **325**(5947): p. 1513-1515.

48. Martin, D., "All-Optical Computers" Could Soon be a Part of Our Life. http://www.uofaweb.ualberta.ca/researchandstudents/news.cfm?story=53318, 2006.

CHAPTER 3 OPTICAL SIMULATION OF 3D SPIRAL PHOTONIC CRYSTALS

The commercial software package OptiFDTD was used to simulate the response to circularly polarized light of 3D spiral PhCs. The simulation results can guide the fabrication to produce appropriate structures. OptiFDTD is mainly based on the finite difference time-domain (FDTD) method. Therefore, we briefly introduce the basics of FDTD in section 3.1. In section 3.2, optical transmittance spectra of 3D spiral PhCs fabricated by transparent materials are calculated based on different RI contrast and pitch numbers. Both LCP and RCP incident light are used. Dispersive material like aluminum as another type of material is investigated in section 3.3. Section 3.4 will summarize conclusions.

3.1 Introduction of FDTD

The FDTD method is used for simulating optical performance of diffractive optic devices [1, 2]. It has the capacity to model light propagation, reflection and polarization effects of optic devices. The essence of the FDTD approach is to solve time-dependent Maxwell's curl equations. For 3D simulations, a cubic box will be chosen as the calculation boundary. This cubic box is meshed in the space domain as shown in FIGURE 3.1. Both electrical and magnetic field are represented by a 3D array --- $E_x(i, j, k)$, $E_y(i, j, k)$, $E_z(i, j, k)$, $H_x(i, j, k)$, $H_y(i, j, k)$, $H_z(i, j, k)$. Note that the E and H components are interleaved at intervals of $\frac{1}{2}\Delta h$ in space and $\frac{1}{2}\Delta t$ in time for implementing a leapfrog algorithm. The new value of H and E field are calculated based on the old value of H and E field. The initial field will be introduced on the left boundary. By using discrete equations derived from Maxwell's curl equations, all area's E and H field can be derived step by step using step spacing.

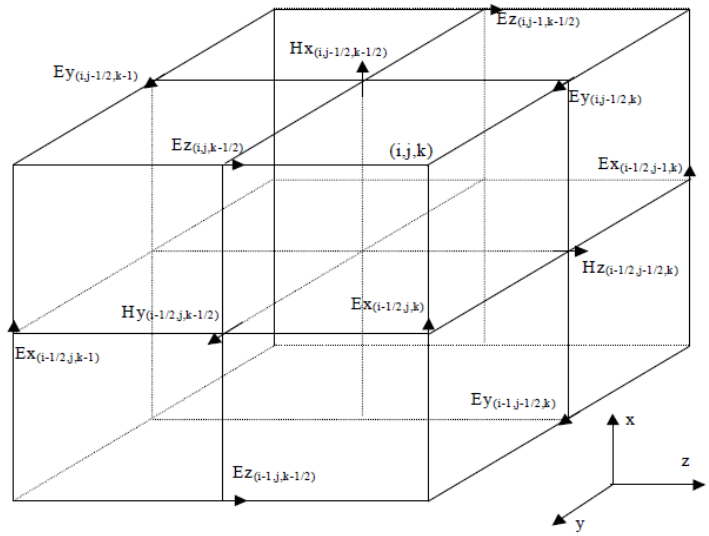

FIGURE 3.1 Displacement of the electric and magnetic field vector components about a cubic unit cell of the Yee space lattice [3].

To maintain the accuracy, numerical dispersion and the stability of the FDTD method, the step size for the time and space are constrained by equation 3.1 and 3.2 respectively [3].

$$\min\text{imum}(\Delta x, \Delta y, \Delta z) \leq \frac{\lambda_{\min}}{10 n_{\max}} \tag{3.1}$$

$$\Delta t \leq \frac{1}{v\sqrt{\frac{1}{(\Delta x)^2}+\frac{1}{(\Delta y)^2}+\frac{1}{(\Delta z)^2}}} \tag{3.2}$$

In equation 3.1 and 3.2, v refers to the speed of light in the dielectric materials and $n_{\max}$ is the maximum RI value in the computational domain. Also, the refractive index in FDTD algorithm is independent on the size. Therefore, whenever size features are small enough to comparable with the Debye length, FDTD simulation breaks down.

3.2 Optical transmittance of 3D spiral PhCs

3.2.1 Optical transmittance of 3D spiral PhCs with different RI contrast

Photoresist SU-8 and As_2S_3 have been chosen for optical transmittance calculations. Like most other photoresist, the RI of the SU-8 is around 1.5. During the simulation process, RI of SU-8 is *1.54+0.002i* while As_2S_3 's is *2.45+0.002i*. The imaginary part of complex index refers to the absorption coefficient. The excitation sources are LCP and RCP light respectively. The schematic diagram of the optical simulation for 3D spiral structures is shown in FIGURE 3.2.

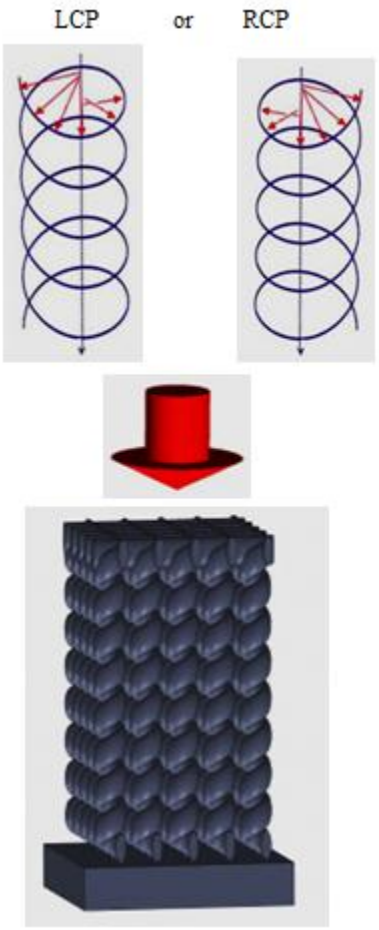

FIGURE 3.2 Schematic of optical simulation for 3D spiral structures.

In order to calculate a broad wavelength range excitation source, a Gaussian-distributed pulsed light source is used. Its mathematical expression can be written as

$$T(t) = \exp[-\frac{1}{2}\left(\frac{t - t_{off}}{t_w}\right)^2 \sin(\omega t) \tag{3.3}$$

where t_{off} is the offset time, t_w is the half width of the pulse, and ω is the central frequency of the excitation light.

FIGURE 3.3 shows the schematic diagram of 3D spiral PhCs. By utilizing the scalability of PhCs, we choose the feature sizes of the simulated structures smaller than the as-fabricated structures for the purpose of shifting the operation wavelength close to visible light regime. For the structure parameters, DW, NS, SG, LP and DS refer to the diameter of spiral wires, the number of spiral turns, the spacing of the grid, the length of spiral pitches and the diameter of spiral structures respectively. The structures with DW=390nm, NS=8, SG=1.3μm, LP=1.3 μm and DS=780nm are used for numerical simulation.

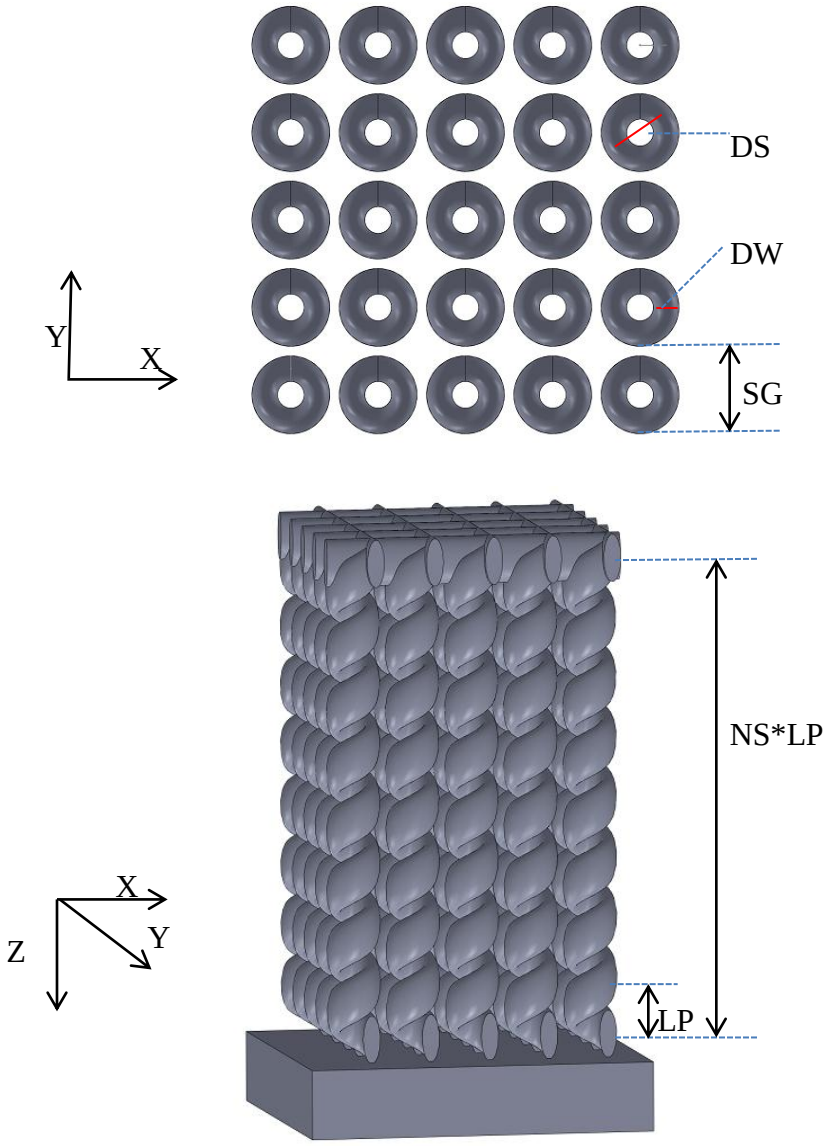

FIGURE 3.3 Front and side view of 3D spiral PhCs for numerical simulations.

The basic FDTD method needed to be modified at the boundaries of computational domain. The boundaries along X and Y directions were simulated by periodic boundary conditions (PBC) [4] because of the structure periodicity. The boundary along the Z direction was perfectly matched layers (PBL) [5] to prevent the incident wave reflecting from interface.

For the spiral structures, the spiral shape couldn't be directly drawn through the OptiFDTD software. The software only provides four basic 3D shapes: sphere, cylinder, ellipsoid, and block. The basic ellipsoid is used by following the trajectory of a 3D spiral PhCs to draw simulated structures with the help of VB script. This process is exactly the same as the fabrication process through point-by-point scanning writing in the LDW system. The shape of the small focal volume in the LDW system is also ellipsoid. The detailed code programmed by VB script is listed in Appendix A. In order to save computer memory and increase simulation speed, 64 bit simulator and 64 bit personal computer have been chosen for computational simulation.

The layout of 3D spiral structures in OptiFDTD is shown in FIGURE 3.4. The input field is the element to define the incident light. Observation point is used to record the data like electric or magnetic field at the desired point. Like the observation point, the observation area can record the data in the interested area. Also, it can be used to calculate the transmittance and reflectance of a designed structure. Spacing in the x, y and z directions is chosen as 50 nm. The time step is chosen 0.08329fs. Both space and time steps are chosen reasonably to meet equations (3.1) and (3.2), respectively. The total calculation domain is 18 μm by 1.3 μm by 1.3 μm.

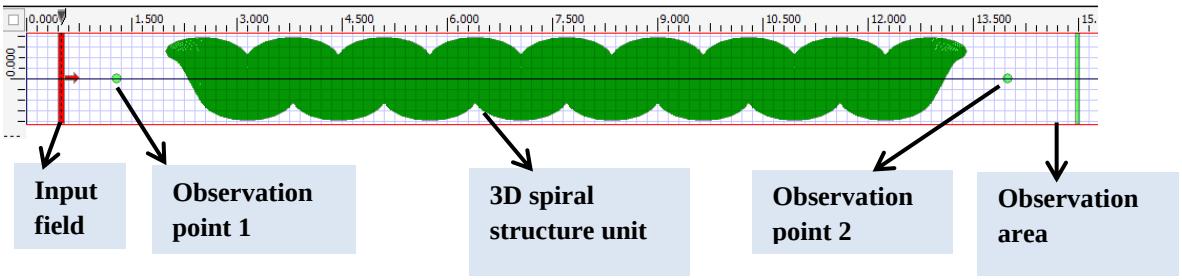

FIGURE 3.4 The layout of 3D spiral structures in OptiFDTD.

After setting up refractive index, structure parameters, excitation source, mesh size and boundaries of the computation domain, we get the optical transmittance of 3D spiral PhCs based on SU-8 and As_2S_3 as shown in FIGURE 3.5. The SU-8 and As_2S_3 are two photorests we have used for microstructure fabrication.

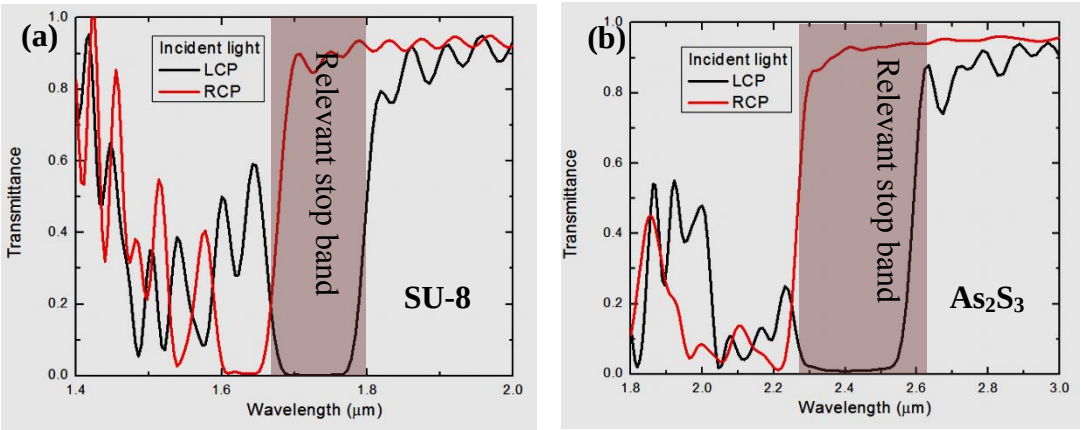

FIGURE 3.5 Calculated optical transmittance of 3D spiral structures for (a) SU-8 and (b) As_2S_3.

Both FIGURE 3.5(a) and (b) represent the circular polarization effect. Compared with SU-8, 3D spiral PhCs based on As_2S_3 show broader circular polarization over larger wavelength range since they a broader so-called "stop band". The conclusion is consistent with the theory of cholesteric liquid crystal structure. In cholesteric liquid crystal structure , the center operation wavelength $\lambda_0 = p * n$ while the operation bandwidth $\Delta\lambda = p * \Delta n$, where Δn is the refractive index contrast in parallel and perpendicular direction. The stop band in FIGURE 3.5 is determined by the extension ratio which is defined by the ratio between two incident lights' optical transmittances. When the ratio is above the exponential value e, we consider the 3D spiral PhCs have circular polarization effect in this specific wavelength. In addition, the relevant stop band blue-shifts with the increased RI.

For As_2S_3, the wavelength of 2.4 μm has the most effective polarization effect. The light propagation in this wavelength point is simulated in FIGURE 3.6 to show the electric field differences in the y direction (Ey) for two orthogonal lights. The left-handed 3D spiral PhCs can pass the RCP light while it forbids or reflects the LCP light. The electric field intensity versus running time for two different positions is shown in Figure 3.7. Compared with the RCP light, the LCP light is strongly suppressed after it passes through the 3D spiral structures.

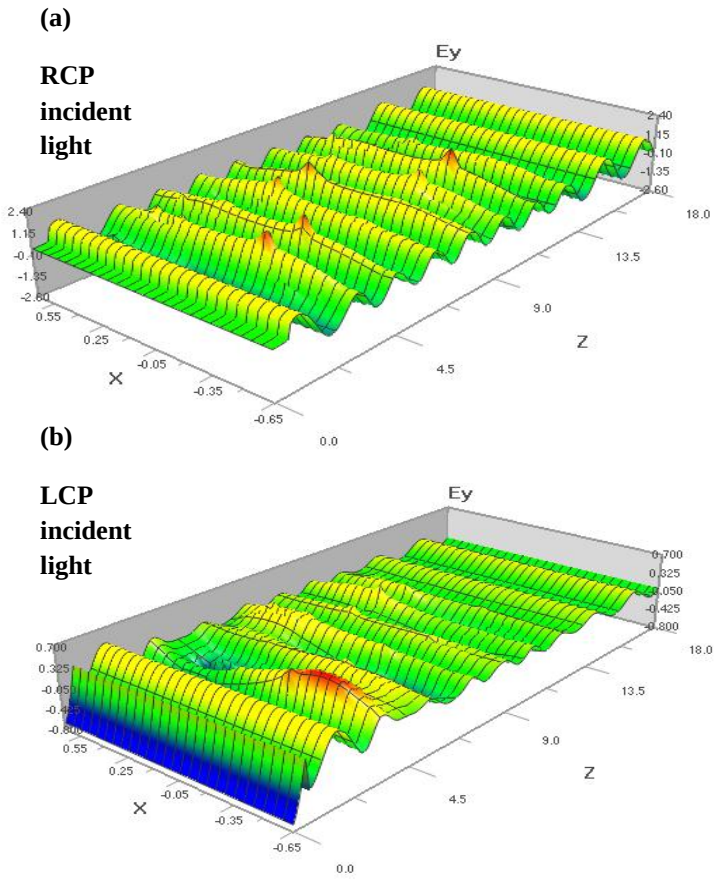

Figure 3.6 Light propagation for RCP and LCP incident light in As_2S_3 3D spiral structures. Ey denotes the electric field in y direction.

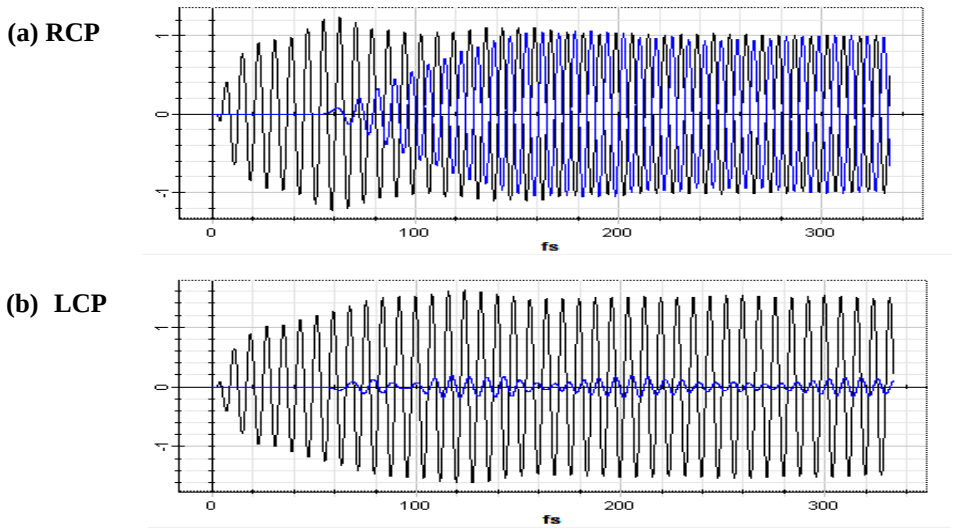

Figure 3.7 Ey intensity vs time in different observation point. The dark profile is for observation point 1 while the blue one is for observation 2. These two points are before and behind the 3D spiral structures respectively.

3.2.2 Optical transmittance of 3D spiral PhCs with different pitch numbers

Except for the RI contrast, the pitch numbers of the 3D spiral PhCs are another important factor for affecting the circular polarization effect. Based on the same structure parameters we used above for the RI contrast investigation, we investigated the pitch number of 1, 2, 4 and 6. FIGURE 3.8 shows different transmittance spectra based on the pitch numbers. The increased pitch numbers will establish the polarization effect since the spiral structure provides the necessary pathway for interaction with light. FIGURE 3.8 has proved this assumption and also demonstrated that the polarization effect has almost reached the maximum performance when the pitch number is 6. Also, the center operation wavelength λ_0 is fixed which is consistent to the equation: $\lambda_0 = \mathrm{p} * \mathrm{n}$.

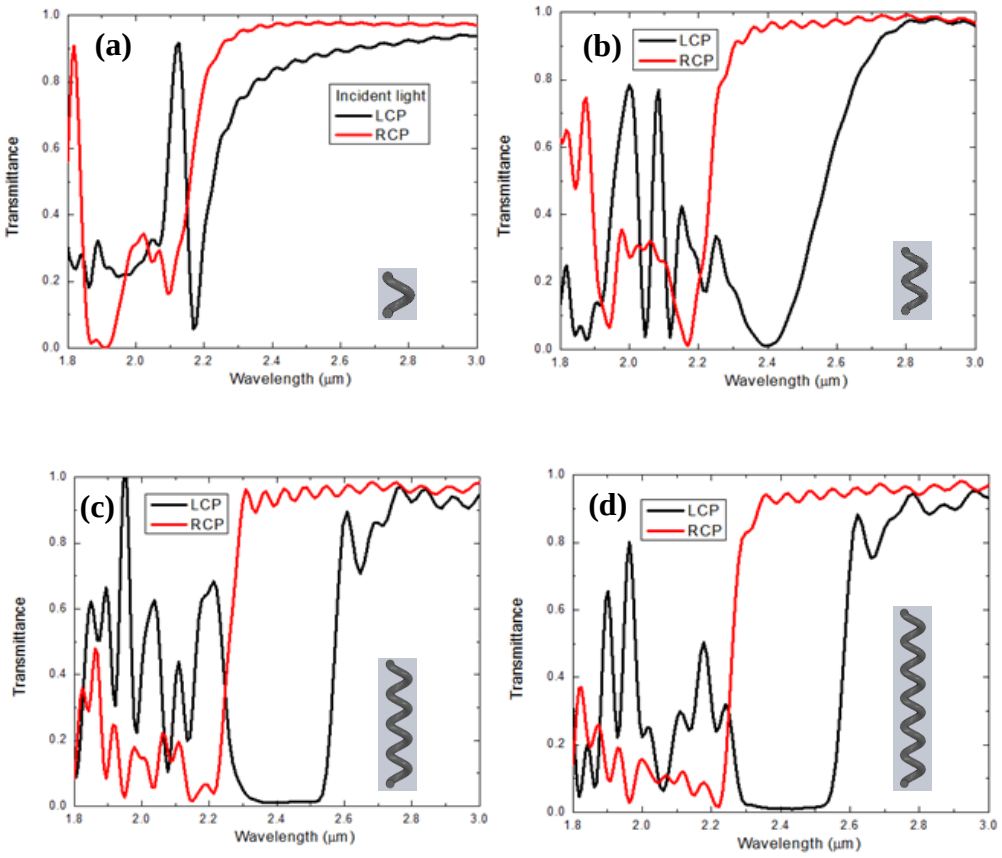

FIGURE 3.8 Polarization selection effect of 3D spiral PhCs with different pitch numbers: 1, 2, 4 and 4 respectively.

3.3 Optical transmittance of dispersive material

Metal materials can be a good candidate for fabricating 3D spirals PhCs as circular polarizers. Broadband circular polarizers based on metal 3D spiral photonic crystals have been fabricated [6]. In a single metal helix, the internal resonance of an individual metal helix will lead to a narrow frequency response. Also, the Bragg resonances originating from PhCs can also exhibit a narrow frequency response. The combination of these two effects, however, can lead to a broadband circular polarizer.

Aluminum (Al) as a dispersive material was used for optical transmittance calculation of 3D spiral PhCs. During the simulation process, a Lorentz-Drude model as represented in

Eq. (3.3) was used for precisely describing the metal's dielectric function by Lorentz-Drude model. This form separated explicitly the intraband effects (also referred to as free electron effects) from interband effect (also referred to as bound-electron effects). The intraband part $\varepsilon_r^f(\omega)$ is described by the well-known Drude model while the bound-electron part $\varepsilon_r^b(\omega)$ is presented by Lorentz model.

$$\varepsilon_r(\omega) = \varepsilon_r^f(\omega) + \varepsilon_r^b(\omega) = [1 - \frac{\Omega^2}{\omega(\omega - i\Gamma_0)}] + [\sum_{j=1}^{k} \frac{f_j \omega_p^2}{(\omega_j^2 - \omega^2) + i\omega\Gamma_j}] \tag{3.3}$$

In Eq. (3.3), ω_p is the plasma frequency associated with intraband transitions with oscillator strength f_0 and damping constant Γ_0; k is the number of oscillators related to the frequency ω_j, strength f_j and the lifetime $1/\Gamma_j$.

The structure parameters used in Ref. (7) have been chosen for validating our simulation results. Two types of structures have been studied: single-helix and double-helix. Following the structure parameter definition in section 4.2.1, we have chosen DW=50nm, NS=3, SG=190nm, LP=200nm and DS=100nm. The specific parameters of Lorentz-Drude are quoted from Ref. (3) and (8).

The optical transmittances of single- and double-helix 3D spiral PhCs for Al is presented in FIGURE 3.9. The blue line represents polarization suppression ratio between LCP and RCP transmittance. The simulation wavelength range is from 0.4μm to 1.8μm. It shows that the operation band can be increased by increasing one more helix in each individual unit. This is because denser Al material can interact with incident light more efficiently. These results are consistent with Ref. (8).

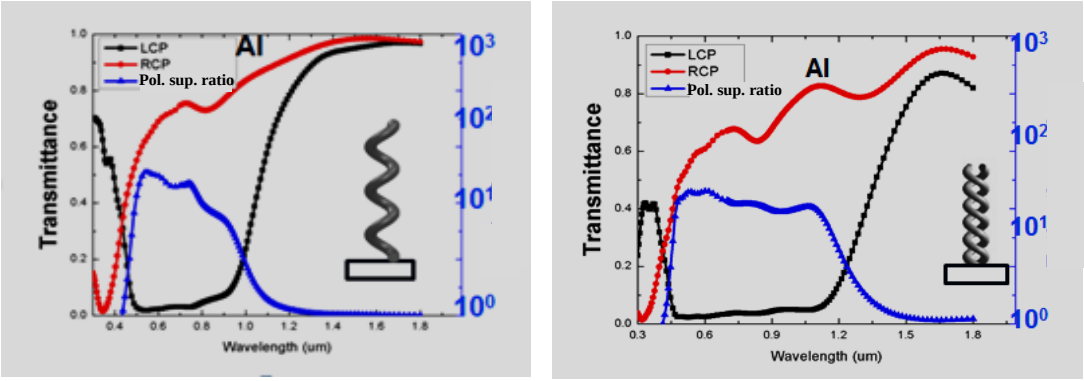

FIGURE 3.9 Optical transmittances of single- and double- helix 3D spiral PhC for Al.

3.4 Conclusions

The FDTD method is a very powerful simulation tool for designing and investigating the optical performances of the optical devices. In our simulation work, we attempted to obtain the optical transmittance of 3D spiral PhCs. Three-dimensional spiral structures were approximated by a series of ellipsoids by following spiral trajectory. The simulation results showed that 3D spiral PhCs possess circular polarization effect for both low and high RI materials. Higher refractive index materials provide broader stop bands ($\Delta\lambda$ increases). Also, the electrical field intensity distribution for both LCP and RCP waves was obtained to further prove 3D spiral structure's polarization effect. Furthermore, an absorptive (metal) for potential use as a broadband circular polarizer was investigated. The simulation results of Al material showed the denser structure with double helix in each unit had broader operation wavelength then the single-helix 3D spiral PhC but results in lower polarization selection ratios than for the dielectric structure.

References

1. Lavrinenko, A., et al., *Comprehensive FDTD modelling of photonic crystal waveguide components.* Optics Express, 2004. **12**(2): p. 234-248.

2. Kosmidou, E.P., E.E. Kriezis, and T.D. Tsiboukis, *FDTD analysis of photonic crystal defect layers filled with liquid crystals.* Optical and Quantum Electronics, 2005. **37**(1-3): p. 149-160.

3. OptiFDTD Technical Background and tutorials, version 7.0, Optiwave, Inc.

4. Holter, H. and H. Steyskal, *Infinite phased-array analysis using FDTD periodic boundary conditions - Pulse scanning in oblique directions.* IEEE Transactions on Antennas and Propagation, 1999. **47**(10): p. 1508-1514.

5. Gedney, S.D., *An anisotropic perfectly matched layer-absorbing medium for the truncation of FDTD lattices.* IEEE Transactions on Antennas and Propagation, 1996. **44**(12): p. 1630-1639.

6. Gansel, J.K., et al., *Gold Helix Photonic Metamaterial as Broadband Circular Polarizer.* Science, 2009. **325**(5947): p. 1513-1515.

7. Yang, Z.Y., et al., *Ultrabroadband optical circular polarizers consisting of double-helical nanowire structures.* Optics Letters, 2010. **35**(15): p. 2588-2590.

8. Rakic, A.D., et al., *Optical properties of metallic films for vertical-cavity optoelectronic devices.* Applied Optics, 1998. **37**(22): p. 5271-5283.

CHAPTER 4 FABRICATION OF 3D SPIRAL PHOTONIC CRYSTALS

Three dimensional PhCs are artificial materials which have periodically varing refractive index (RI) for localizing and guiding the light propagation. The concept of 3D PhCs has been proposed more than 20 years ago [1, 2]. However, the fabrication of arbitrary structures with relatively high RI is still a big challenge. The self-assembly method and holographic laser lithography discussed in Chapter 2 are restricted to a few structures with "high symmetry" like the face-centered cubic. The layer-by-layer method with alternate repetition of deposition and etching required high-precision alignment and long fabrication time. In our work, in order to avoid these disadvantage, we adapted direct laser writing system (LDW) to fabricate 3D spiral PhCs with desired structure parameters. Compared with other fabrication methods, the LDW system could write arbitrary structures based on point-to-point scanning. Furthermore, arsenic-sulfide (As_2S_3) glasses have been used for 3D spiral PhCs because of their dual advantages: high RI and strong mechanical support. Usually, the RI of photo-resist is as low as 1.5 while As_2S_3 has RI up to 2.5 which can strongly modulate light propagation to obtain complete photonic band gap and broad operation wavelength for circular polarization selection.

In this work, the fabrication of high quality 3D spiral PhCs with high RI will be demonstrated. The FIGURE 4.1 describes the fabrication processes. The first step is the thermal evaporation with a source temperature below 390℃. As_2S_3 will evaporate and deposit on a glass substrate. In the second step, LDW system locally exposes the photoresist prepared by the thermal evaporation deposition. With two-photon absorption (TPA), a selective etching rate between the exposed and unexposed areas will result.

Finally, wet etching with higher etching rate of the unexposed area will reveal 3D spiral structures.

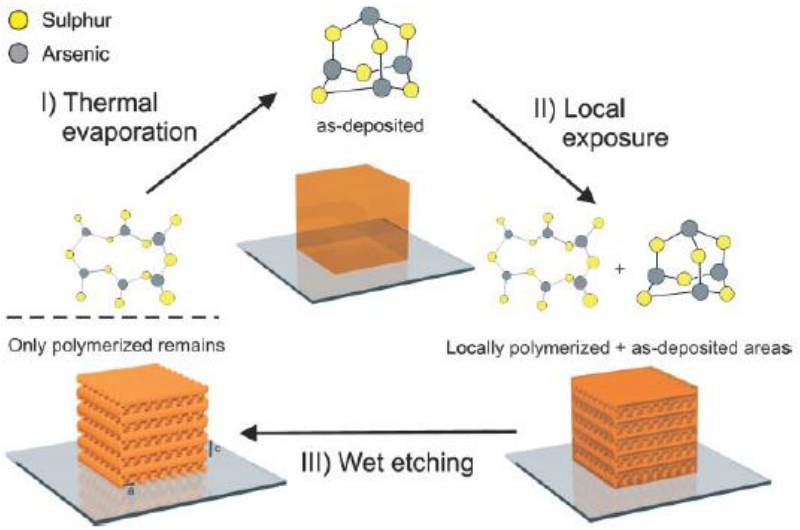

FIGURE 4.1 The three fabrication steps [3]. 1) Thermal evaporation of glassy As2S3 2) Direct writing system exposes photoresist in desired place 3) Removal of unexposed photo-resist to obtain 3D spiral PhCs.

We will briefly discuss thermal evaporation deposition in section 4.1. In section 4.2, the mechanism of the LDW system will be introduced. Two-photon absorption as a crucial part of LDW system will be explained. Wet etching will be presented in section 4.3. Together with these three sections, high-quality 3D spiral PhCs will be presented and discussed in section 4.4 with SEM micrographs.

4.1 Thermal evaporation deposition

In this work, 10 μm thick As_2S_3 as photoresist was prepared by thermal evaporation. The thickness of As_2S_3 photoresist was measured by XP series stylus profilers (AMBios technology Inc.). Solid glassy As_2S_3 (Amorphous Materials Inc.) was used as the precursor material. Silica glass coverslips of 30 mm diameter (Warner Instruments, 170

μm) were used as substrates. The diameter of the silica glass substrate was perfectly matched to the substrate holder in the LDW system while the 170 μm thickness was used for adapting the working distance of the optical microscopy. For accommodating the size of the sample holder of the thermal vapor evaporation chamber, the glassy As_2S_3 was mashed into small pieces by a hammer. Through thermal evaporation at a temperature of 380℃, the glassy As_2S_3 was converted to As_4S_6. A high content of As_4S_6 is desirable to obtain two-photo absorption [3, 4]. The vacuum pressure of the evaporation chamber was maintained around $6-8\times10^{-6}$ torr. The deposition rate was controlled by adjusting evaporation temperature and measured with a quartz microbalance. The whole process for As_2S_3 preparation takes around two hours. FIGURE 4.2 shows that the as-deposited photoresist is orange and transparent.

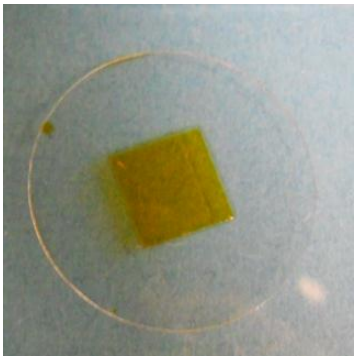

FIGURE 4.2 As_2S_3 photoresist produced by thermal vapor deposition.

4.2 Laser direct writing system

4.2.1 Two-photon absorption effect

The essence of the LDW system is two-photon absorption (TPA). Compared with a conventional lithography system, which can fabricate two-dimensional patterns, LDW system can write almost arbitrary micro-structures. In FIGURE 4.3, the photoresist simultaneously absorbs two near-infrared (IR) photons whose collective energy is equal

to an ultraviolet photon [5]. The rate of the TPA is proportional to the square of the light intensity which causes that TPA mainly occurs around the laser focal point. The linear relationship between TPA and the quadratic light intensity causes the TPA area size beyond the diffraction limit of the incident light wavelength.

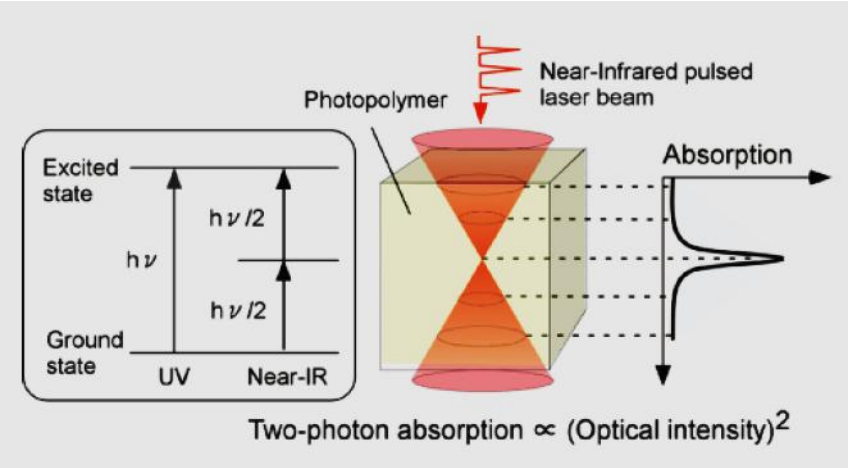

FIGURE 4.3 Two-photon polymerization induced by a focused laser beam [5].

FIGURE 4.4 is the optical absorption spectrum of an unexposed SU-8 film. Without TPA, SU-8 film has negligible absorption in the near-IR regime. After TPA, the absorption intensity can be reached close to the absorbance peak around the UV regime where the laser beam is tightly focused into a tiny volume.

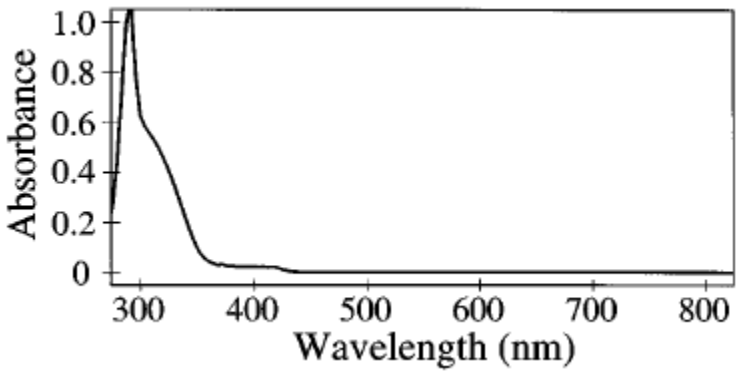

FIGURE 4.4 Optical absorption spectrum of an unexposed SU-8 film [6].

With the capability of 3D micro-fabrication and submicron resolution, TPA is widely used for fluorescence image techniques [7], 3D data storage [8] and 3D micro-fabrication [3, 9-10].

Arbitrary structures can be fabricated by a LDW system because it exposes a very small point each time. By moving the relative position between the laser focal point and the photoresist, we can draw any desired pattern by point-by-point scanning. FIGURE 4.5 presents different 3D microstructures fabricated by a LDW system.

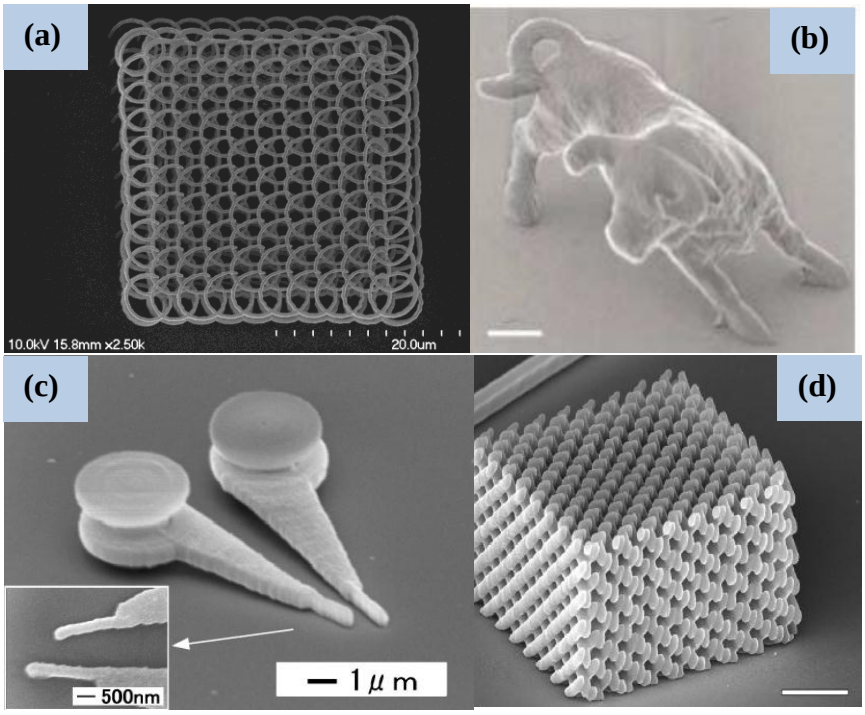

FIGURE 4.5 Different 3D microstructures fabricated by two-photo polymerization. (a) connected spiral PhCs in IP-L material. (b) micron bull [11]. Scale bar, 2 μm (c) microtweezers with submicron probe tips [12] (d) slanted pore PhCs [13]. Scale bar, 3 μm.

4.2.2 Laser direct writing system

Photonic Professional system (Nanoscribe GmbH) is the commercial LDW system used for 3D micro-structure fabrication in this work. The whole system as shown in FIGURE 4.6 was located in a yellow light room for preventing unintentional light exposure. It consists of three elements: the laser and optics cabinet, the inverse microscope and the electronic rack. The laser source provides short pulses (around 150fs) at a center wavelength of 780nm ±10nm. The repetition rate of the laser is 100MHz. Even though the single pulse peak power is very high, the average light power is low (100mW) because the total pulse width of the single pulse is five orders of magnitude higher than the single pulse. The sample is mounted on a computer controlled three-axes piezo electrical scanning stage. The piezo range is $300\,\mu m \times 300\,\mu m \times 300\,\mu m$. That's the maximum size of the fabricated structures without the help of the motorized scanning stage. An acousto optic modulator (AOM) controlled by the computer can adjust the laser intensity. The light pulses are tightly focused into the As_2S_3 as photoresist by a 100× oil immersion objective with high numerical aperture (NA=1.4). The expansion lens expands the laser beam size to match the oil objective size.

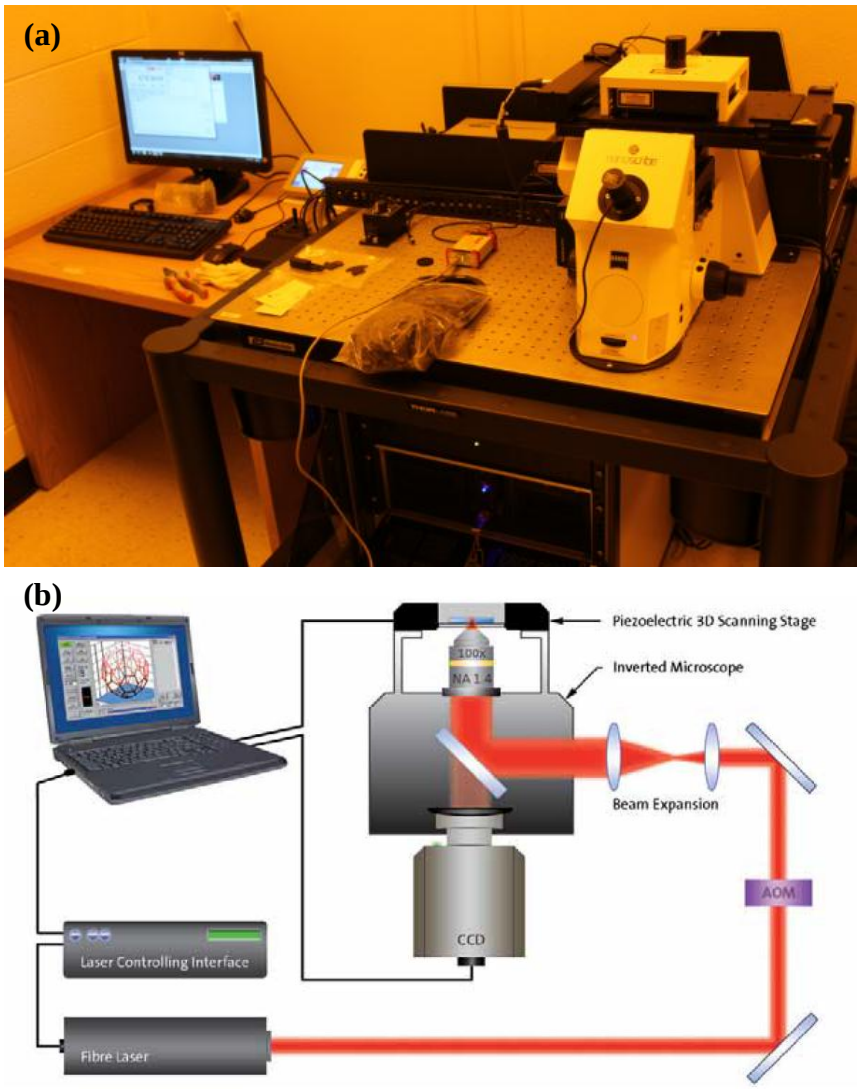

FIGURE 4.6 Nanoscribe Photonic Professional system: (a) LDW system in the yellow light room, (b) diagram of all main components.

Influence of the index mismatch on the voxel shape of the laser beam becomes significant because the RI of As_2S_3 photoresist is very high [3]. Intuitively, the rays will be refracted in the interface between As_2S_3 photoresist and glass substrate as shown in FIGURE 4.7. Without defocus factor adjustment, the discrepancy between the actual and intended writing position will vary a lot. The defocus factor is chosen as 0.62 by referring the relationship between the defocus factor and the RI of the refraction [14].

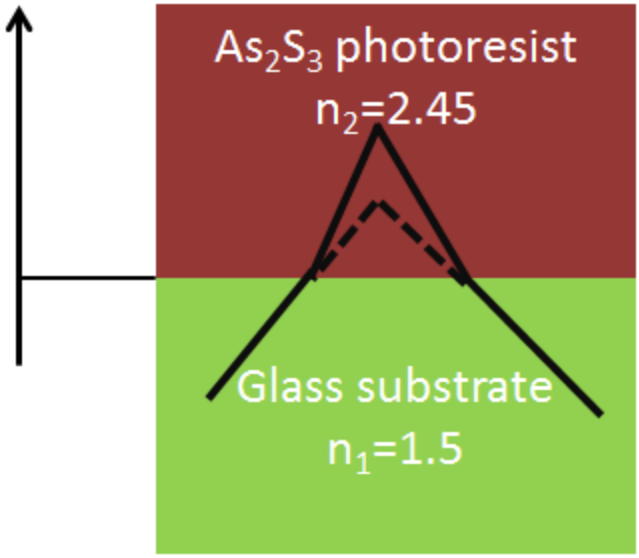

FIGURE 4.7 Focus point influence of the index mismatch.

The GWL script language is used in the LDW system to maximize the flexibility of the writing process. Laser power, focus place, point distance, writing speed and other related writing parameters can be defined by GWL language. Also, GWL working together with Matlab or Labview software can easily generate the codes for any specific structures' writing. The GWL script of the spiral 3D PhCs is attached in Appendix B.

4.3 Wet etching

After the laser exposure by LDW system, the development solution is used to remove the unexposed area. Diisopentylamine (Alfa Aesar) with concentrations between 0.05% to 3 mol-% was used. Diisopentylamine slowly dissolves the exposed areas (crosslinked As_2S_3) while rapidly dissolving unexposed area which is mainly As_4S_6. Another liquid, dimenthylsulfoxide, is used to dilute the diisopentylamine. As high concentration of

diisopentylamine etches the sample too rapidly which can ultimately cause the sample to peel off the glass substrate; while a low concentration doesn't dissolve the unexposed area. Different concentrations of diisopentylamines are tested to optimize the etching speed. Finally, we found 0.5mol-% diisopentylamine solution is an optimized development solution.

The wet etching process requires a clean substrate. Otherwise, the glassy As_2S_3 photoresist easily peels off from the glass substrate during the wet etching process. Figure 4.8 shows a homemade glass substrate holder for cleaning. Three solutions: acetone, isopropanol alcohol and deionized water were used sequentially for ten minutes in ultrasonic device to clean the glass substrate.

Figure 4.8 Homemade glass substrate holder.

4.4 Results and discussions of the as-fabricated 3D spiral PhCs

To obtain high-quality of 3D spiral PhCs, several factors are crucial. Laser power, defocus factor, structure size, etching time and development solutions were investigated.

4.4.1 3D spiral PhCs produced with different laser power

As_2S_3 material was used to fabricate the same size spiral structures with different laser power. Laser powers of 7.8, 6.6 and 5.4mW were used. In Figure 4.9, 7.8mW laser power exposed more area than the design area because of the increased focal volume caused by

increased laser power. 5.4mW laser power in Figure 4.9 (c) was too small to expose the focal point fully. As a result, some places in the exposed area were also washed away by the development solution. Figure 4.9 (d) is the close-up of Figure 4.9 (c). The spiral was split into several branches because of over-etching. 6.6 mW laser power can produce best spiral structures among these three powers.

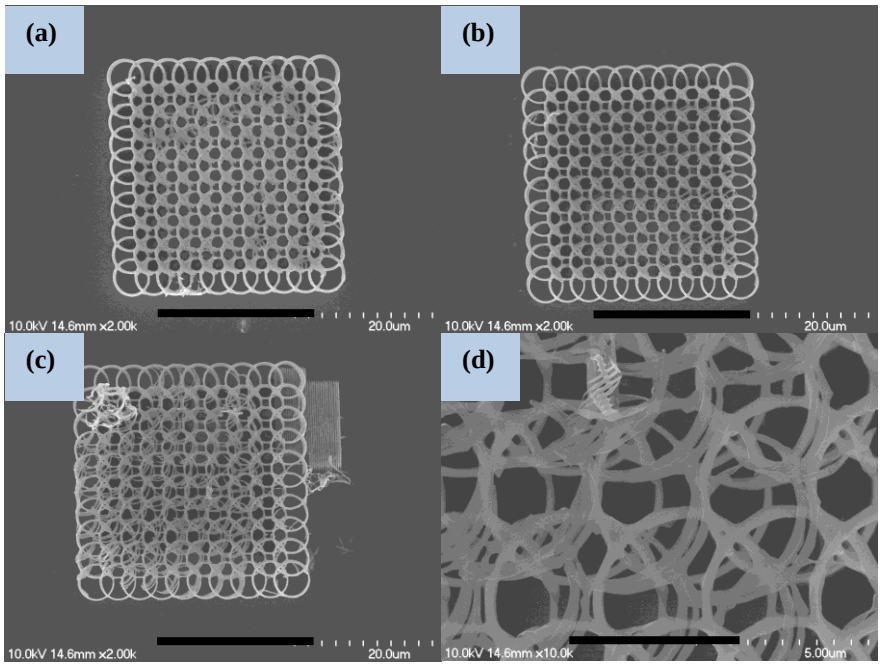

Figure 4.9 The SEM graphs of 3D spiral structures produced by different laser powers. (a) 7.8 mW, (b) 6.6mW, (c) 5.4 mW, (d) the close-up of (c).Scale bar is 20 μm for (a)-(c) but 5 μm for (d).

4.4.2 3D spiral PhCs produced with different defocus factor

Defocus factor becomes very important when the photoresist has a high RI which can lead to an index mismatch. Compared with the spiral structures in Figure 4.10 (a), the structures in Figure 4.10 (b) has higher resolution because the defocus factor adjustment can effectively avoid the voxel elongation.

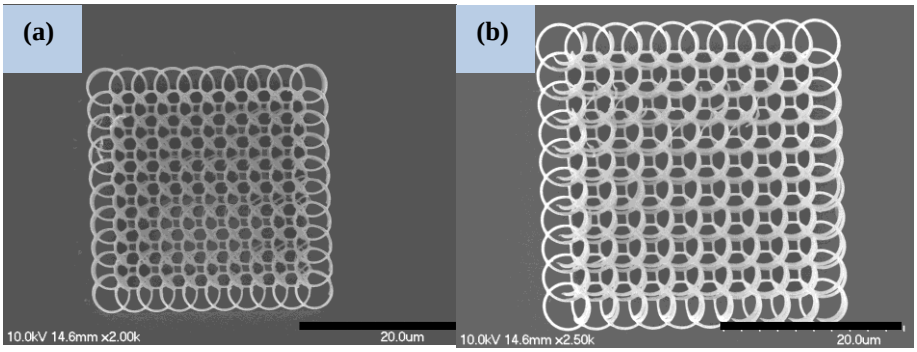

Figure 4.10 Influence of the index mismatch. a) without defocus factor adjustment. b) with defocus factor adjustment.

4.4.3 3D spiral PhCs produced with different etching times

Etching time can directly determine whether the unexposed area is removed thoroughly. FIGURE 4.11 clearly represents the important role of etching time. With proper etching time, 3D spiral PhCs are well revealed. In figure 3.7, 10× 10 spiral structures have lattice constant with 3μm and spiral radius with 2.5 μm. FIGURE 4.11(a), the fabricated structures are not fully revealed because of too short etching time. With longer etching time in FIGURE 4.11(b), the microstructures are clearly revealed.

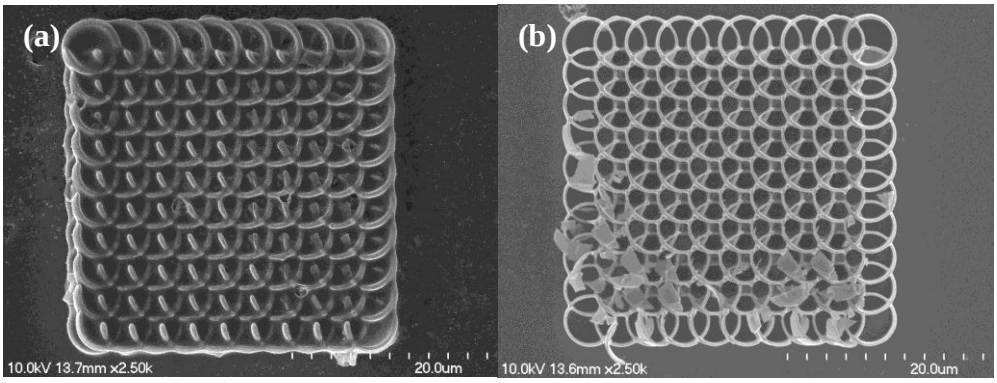

FIGURE 4.11 (a) etching time 10 minutes, (b) etching time 15 minutes. The sample thickness is 10 μm.

4.4.4 3D spiral PhCs produced with different concentrations of development solutions

The concentrations of diisopentylamine solution between 0.05 and 3mol-% were made up to investigate the best concentration for wet etching. We found 0.05mol-% diisopentylamine is too weak to etch the unexposed area while 3mol-% will cause the whole sample fall off from the glass substrate. 0.5mol-% is the best value for wet-etching.

4.4.5 3D spiral PhCs produced with different structure sizes

Through simply adjusting the GWL code, 3D spiral PhCs with different structure sizes were obtained. An etching time of 15mintues yields the best results.

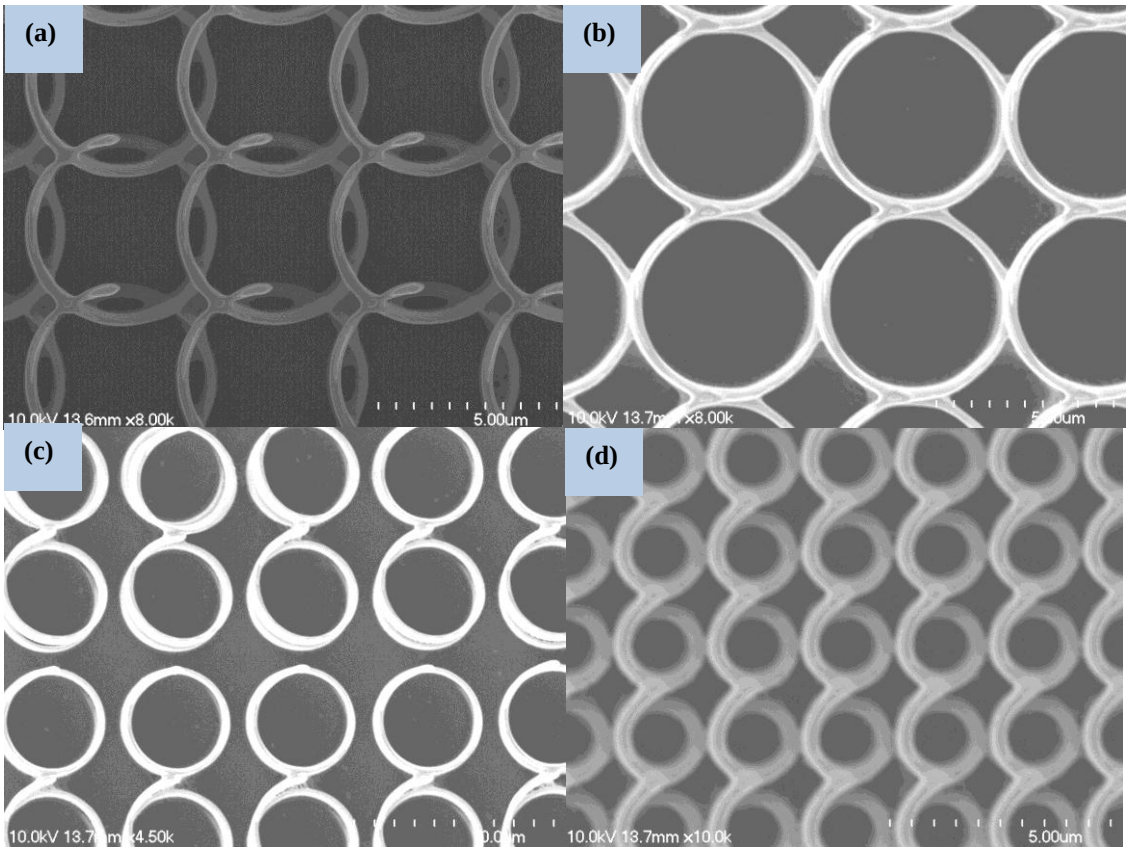

FIGURE 4.12 3D spiral PhCs with different sizes. Lattice constant is denoted as a while the spiral radius is denoted as r here. (a)a=4μm, r=2.5μm; (b) a=5μm, r=2.5μm;(c) a=6μm, r=2.5μm;(d) a=2μm, r=1μm.

By using 4.8mW laser intensity and optimized concentration of wet etching solution, FIGURE 4.12 demonstrates that LDW system has the capability to fabricate arbitrary sizes very easily.

4.4.6 Large size 3D spiral PhCs

In order to implement optical characterization of 3D spiral PhCs , large area size is needed. However, large area size more than 1mm by 1mm takes more than one day to fabricate. Among all structure sizes in section 4.4.5, 2 μm lattice constant was chosen to achieve that the 3D spiral PhCs that can work in a relatively short wavelength regime. In this work, 280μm by 280μm large size area was made for optical characterization. The total writing time by LDW system was around four and half hours. FIGURE 4.13 demonstrates spiral PhCs still maintained very uniform structure throughout the whole area without defects. This is a big advantage over self-assembly. Usually in self-assembly it is almost impossible to maintain defect-free structure over a large area.

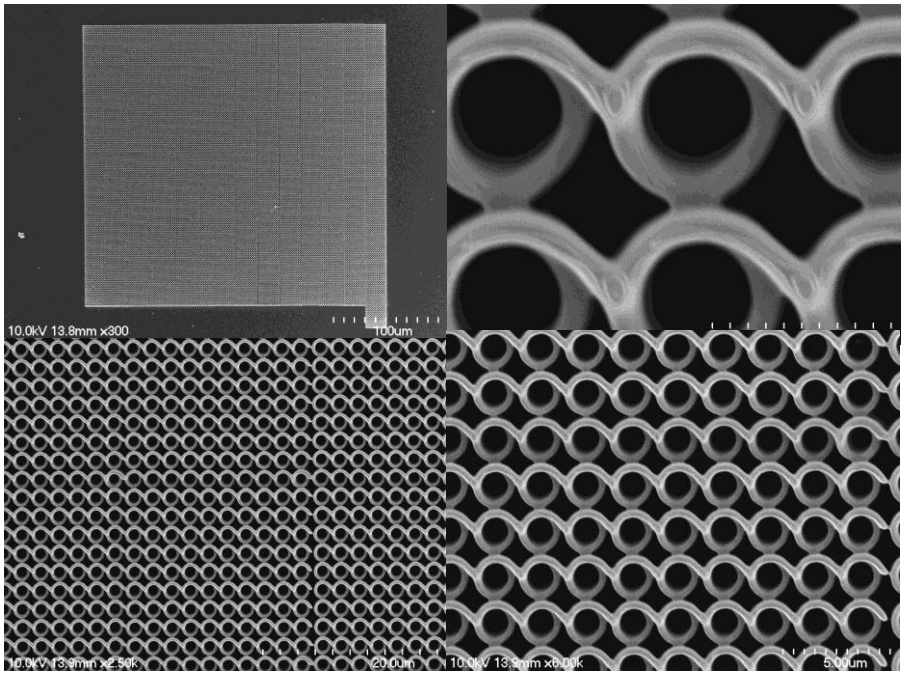

FIGURE 4.13 Large area size of 3D spiral structures.

By tilting the sample stage of SEM system with 35°, we can observe the vertical topology of 3D spiral structures. FIGURE 4.14 shows the uniform 3D structures with two connected neighboring pitches.

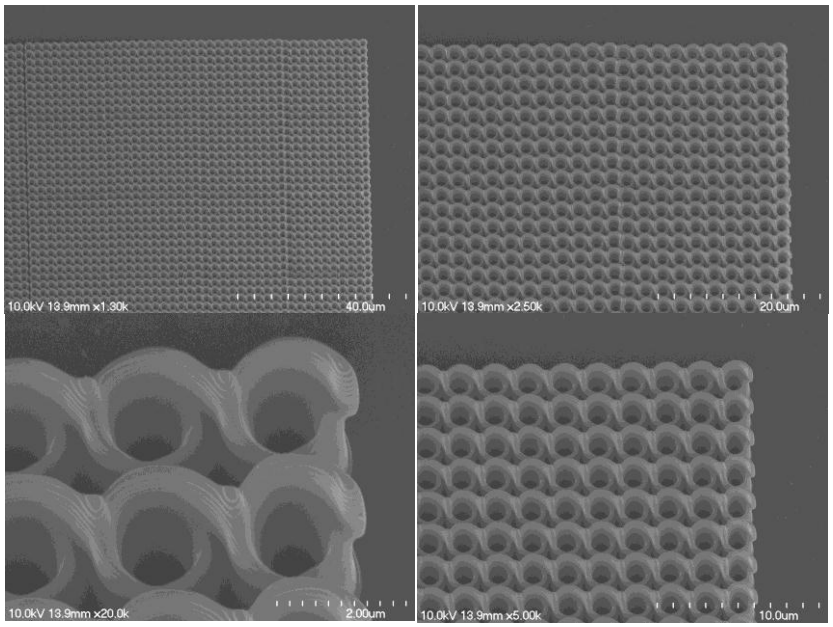

FIGURE 4.14 SEM graphs of 3D spiral structures with 35 ° tilt angle of sample stage of SEM system.

4.4.7 3D spiral PhCs produced based on alternative material: IP-L

As_2S_3 was used for 3D spiral PhCs fabrication above. The LDW system can use many other materials to fabricate microstructures. For example, scaffolds based on Ormocer photoresist were made for cell force measurements [15] in the biotechnology area. Spiral structures fabricated with different sizes in IP-L (Nanoscribe GmbH) are shown in Figure 4.15.

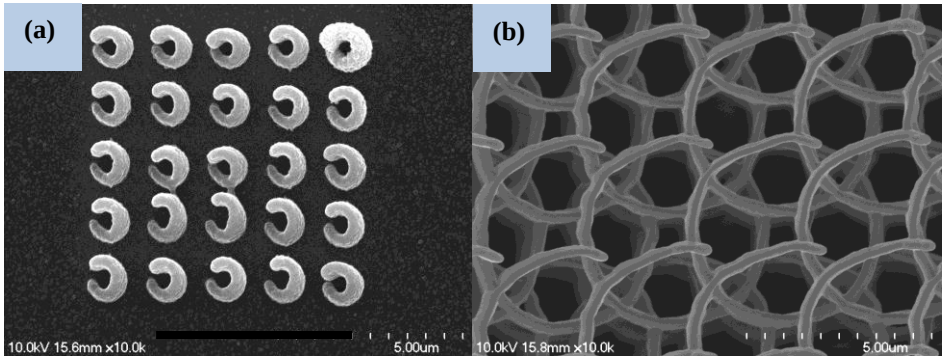

Figure 4.15 Spiral structures fabricated with different sizes in IP-L. (a) Scale bar, 5μm ; (b) Scale bar, 5μm.

4.5 Conclusions

In the fabrication chapter, 3D spiral structures were fabricated by using thermal evaporation, two-photon absorption effect and wet-etching together. Electric current in the vacuum chamber was adjusted to control the deposition rate of the glassy As_2S_3. A quartz microbalance was used to measure the deposition rate. Glassy As_2S_3 with desired thickness can be obtained by adjusting the deposition rate and time.

Computer controlled LDW system can control plenty of writing parameters such as laser power and focal position to obtain optimized writing performance. Almost any arbitrary structures can be fabricated by the LDW system.

During wet etching section, the proper etching time and solution concentration have been chosen to reveal the exposed photo-resist.

References

1. Yablonovitch, E., *Inhibited Spontaneous Emission in Solid-State Physics and Electronics.* Physical Review Letters, 1987. **58**(20): p. 2059.

2. John, S., *Strong localization of photons in certain disordered dielectric superlattices.* Physical Review Letters, 1987. **58**(23): p. 2486.

3. Wong, S., et al., *Direct laser writing of three-dimensional photonic crystals with complete a photonic bandgap in chalcogenide glasses.* Advanced Materials, 2006. 18(3): p. 265-269.

4. Wong, S.H., et al., *Highly selective wet etch for high-resolution three-dimensional nanostructures in arsenic sulfide all-inorganic photoresist.* Chemistry of Materials, 2007. **19**(17): p. 4213-4221.

5. S. Maruo et.al., Laser & Photonics Review. 2, 100 (2008)

6. Witzgall, G., et al., *Single-shot two-photon exposure of commercial photoresist for the production of three-dimensional structures.* Optics Letters, 1998. **23**(22): p. 1745-1747.

7. So, P.T.C., et al., *Two-photon excitation fluorescence microscopy.* Annual Review of Biomedical Engineering, 2000. **2**: p. 399-429.

8. Olson, C.E., M.J.R. Previte, and J.T. Fourkas, *Efficient and robust multiphoton data storage in molecular glasses and highly crosslinked polymers.* Nature Materials, 2002. **1**(4): p. 225-228.

9. Ledermann, A., et al., *Three-dimensional silicon inverse photonic quasicrystals for infrared wavelengths.* Nature Materials, 2006. **5**(12): p. 942-945.

10. Ledermann, A., M. Wegener, and G. von Freymann, *Rhombicuboctahedral Three-Dimensional Photonic Quasicrystals.* Advanced Materials, 2010. **22**(21): p. 2363-2366.

11. Kawata, S., et al., *Finer features for functional microdevices - Micromachines can be created with higher resolution using two-photon absorption.* Nature, 2001. **412**(6848): p. 697-698.

12. Maruo, S., K. Ikuta, and H. Korogi, *Submicron manipulation tools driven by light in a liquid.* Applied Physics Letters, 2003. **82**(1): p. 133-135.

13. Deubel, M., et al., *Direct laser writing and characterization of "Slanted Pore" Photonic Crystals.* Applied Physics Letters, 2004. **85**(11): p. 1895-1897.

14. Nanoscribe Photonic Professional user manual, version 1.4, Nanoscribe GmbH.

15. Klein, F., et al., *Elastic Fully Three-dimensional Microstructure Scaffolds for Cell Force Measurements.* Advanced Materials, 2010. **22**(8): p. 868-871.

CHAPTER 5 CONCLUSIONS AND FUTURE WORK

5.1 Conclusions

Photonic crystals (PhCs) have gone from inception to maturity during the short span of twenty years. Unlike self-assembly and holographic laser lithography methods, laser direct writing (LDW) system can fabricate almost any arbitrary microstructure by programed code control. Three dimensional spiral PhCs used as circular polarizers have been fabricated and simulated in this work. As_2S_3 with a high refractive index has been used in order to create broader circular polarization selection effect.

The results are summarized as follows:

- Simulated the 3D spiral PhCs structures through an ellipsoid approximation by following the spiral trajectory;
- Obtained and investigated optical transmittance of 3D spiral PhCs based on transparent materials with different RI contrast and dispersive material.
- Investigated the writing parameters like laser power, defocus factor, and structure sizes for LDW fabrication;
- Optimized concentration of development solution and etching time for revealing 3D spiral PhCs after laser exposure;

5.2 Future work

Besides fabrication and simulation work, optical characterization by spectrometer is another crucial factor for optical device design. In order to finish optical characterization of 3D spiral PhCs, the test system is expected to meet two requirements: small beam size and circularly polarized light. We plan to set up a characterization system as follows. Lambda 900 spectrometer with the working wavelength range between 170 to 3300nm can be used to measure the optical transmittance spectra. However, Lambda 900

spectrometer couldn’t generate circularly polarized light. Therefore, a linear polarizer and a super-achromatic quarter-wave plate will be installed on the optical bench of Lambda 900 for generating circularly polarized light.

APPENDICES

Appendix A: Transmittance calculation of 3D spiral PhCs by using OptiFDTD 7

OptiFDTD includes three modules: OptiFDTD Designer, OptiFDTD Simulator and OptiFDTD Analyzer [1]. Since OptiFDTD can finish most tasks in OptiFDTD Simulator and Analyzer automatically, we mainly talk about OptiFDTD designer.

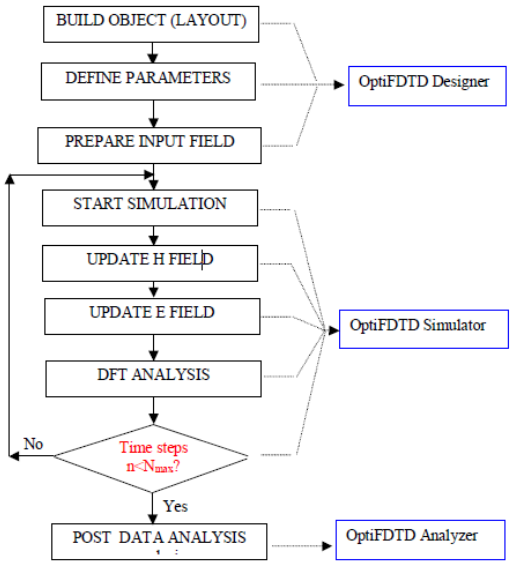

FIGURE A. 1 FDTD simulation flow chart in OptiFDTD [1].

AA. Structure parameters of 3D spiral structures

For the convenience of our simulation work, we set up and change the layouts, materials property, boundary types, excitation sources type, structure size and all other parameters by programming VB code. After running VB code, all structure parameters will be updated based on VB setting-up. The following is an example of VB code we used for transmittance calculation.

VB code:

```
dLh = 1.3                    'Length of the helix pitches
```

```
dPi = 3.14159265358        'PI
dSpace =1.3              'the spacing of the grid
nXdirection = 1           'number of periods (X direction), X+1
nYdirection = 1           'number of periods (Y direction), Y+1
nZdirection = 7           'the number of helix periods (Z direction), Z+1
dRadius = 0.39            'Radius of wire
dDh = 0.39                 'the radius of the helix
Zoffset = 2.5

for X=-(nXdirection-1)/2 to (nXdirection-1)/2
for Y=-(nXdirection-1)/2 to (nXdirection-1)/2
for Z=0 to nZdirection
for m=0.00 to 360 step 360/130

Set Ellipsoid1 = WGMgr.CreateObj ( "WG3DEllipsoid",  "Ellipsoid1"&
Cstr(m)&Cstr(X)&Cstr(Y)&Cstr(Z))

'Set position for Ellipsoid1

Ellipsoid1.SetPosition dSpace*X+dDh*Cos(m*dPi/180),
dSpace*Y+dDh*Sin(m*dPi/180) ,(m/360+Z)*dLh+Zoffset   '   'helical radius is 0.5 ,
helical pitch is 2, left handed

'Set orientation for Ellipsoid1
Ellipsoid1.SetOrientationExpr "", "", ""
Ellipsoid1.SetOrientationOffset    0,    0,    0

'Set clipping plane for Ellipsoid1

Ellipsoid1.SetAExpr "0.19"
Ellipsoid1.SetBExpr "0.19"
Ellipsoid1.SetCExpr "0.513"
'Set material name for Ellipsoid1
Ellipsoid1.SetMaterial "N=1.5"   'Ag-Lorentz-Drude model parameters

next
next
next
next

Dim InputPlane1
Set InputPlane1 = InputPlaneMgr.CreateInputObj ( "Pulse", "Rectangular",
"InputPlane1", "Vertical" )
'Common data for 2D and 3D.
InputPlane1.SetPosition  0.5
InputPlane1.SetDirection "Forward"
```

```
InputPlane1.SetWaveLength "1.6"
InputPlane1.SetTimeHalfWidth "40e-16"
InputPlane1.SetTimeOffset "15e-15"
InputPlane1.SetEnabled  True
'Data for 2D.
InputPlane1.SetAmplitudeOrPower "Amplitude", "1.0"
InputPlane1.SetRefLocal
InputPlane1.SetCenterPos "0.0"
InputPlane1.SetHalfWidth "0.5"
InputPlane1.SetTiltingAngle "0"
'Data for 3D.
InputPlane1.SetAmplitudeExpr3D "1.0"
InputPlane1.SetRefLocal3D
InputPlane1.SetCenterPosExpr3D "0.0", "0.0"
InputPlane1.SetHalfWidthExpr3D "1", "1"
InputPlane1.SetTiltingAngleExpr3D "0"
InputPlane1.SetRHPolarization3D
InputPlane1.RefreshInputField

Dim ObservationPoint1
Set ObservationPoint1 = ObservePtMgr.CreateObservationPoint ( "ObservationPoint1" )
ObservationPoint1.SetCenter  1.3,    0
ObservationPoint1.SetDepthExpr ""
ObservationPoint1.SetEnabled  True
ObservationPoint1.Collect2DTE  False, False
ObservationPoint1.Collect2DTM  False, False
ObservationPoint1.Collect3D  True, True, False, False, False, False

Dim ObservationArea2
Set ObservationArea2 = ObservePtMgr.CreateObservationArea ( "ObservationArea2",
False, False, True )
ObservationArea2.SetCenter   15,    0
ObservationArea2.SetDepthExpr ""
ObservationArea2.SetEnabled  True
ObservationArea2.Collect3D  True, True, True, True, True, True
ObservationArea2.SetWidthOffset  0.000
ObservationArea2.SetHeightOffset  1.300
ObservationArea2.SetWidthExpr  ""
ObservationArea2.SetHeightExpr  ""


Dim ObservationPoint3
Set ObservationPoint3 = ObservePtMgr.CreateObservationPoint ( "ObservationPoint3" )
ObservationPoint3.SetCenter   14,    0
ObservationPoint3.SetDepthExpr ""
ObservationPoint3.SetEnabled  True
```

ObservationPoint3.Collect2DTE False, False
ObservationPoint3.Collect2DTM False, False
ObservationPoint3.Collect3D True, True, False, False, False, False

AB. Simulation parameters set-up

In order to save computer memory and increase simulation speed, 64 bit simulator and 64 bit personal have been chosen for computational simulation. In figure A.2, reasonable parameters have been chosen based on step requirement for both time and space. The number of time steps should be long enough to make sure the incident light's convergence.

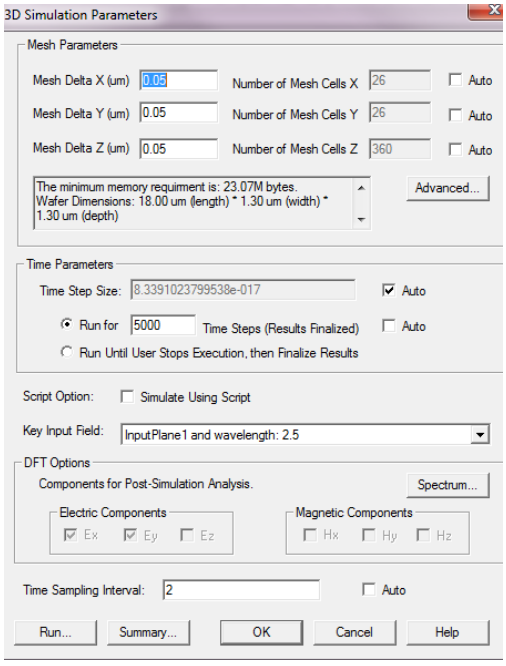

FIGURE A. 2 Simulation parameters set-up.

From Fig. (A.3), we have used the PBC boundaries for x and y directions and PML boundary for z direction.

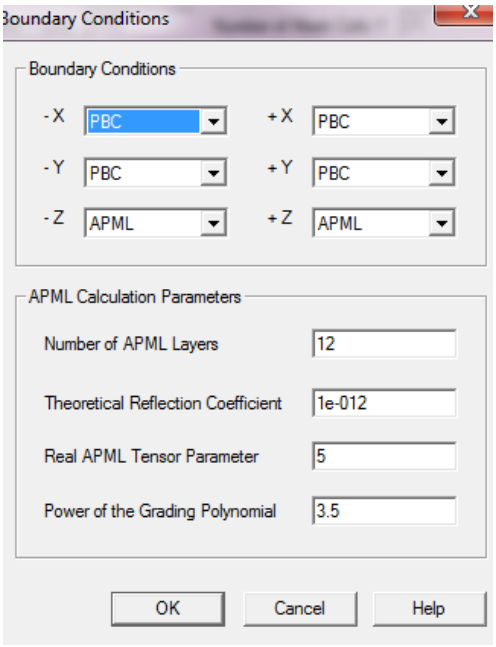

FIGURE A. 3 Boundary conditions setup for all three directions.

After we have set up all design parameters, we open the Design Summary dialog box to review all details of the design as shown in Fig. (A.4).

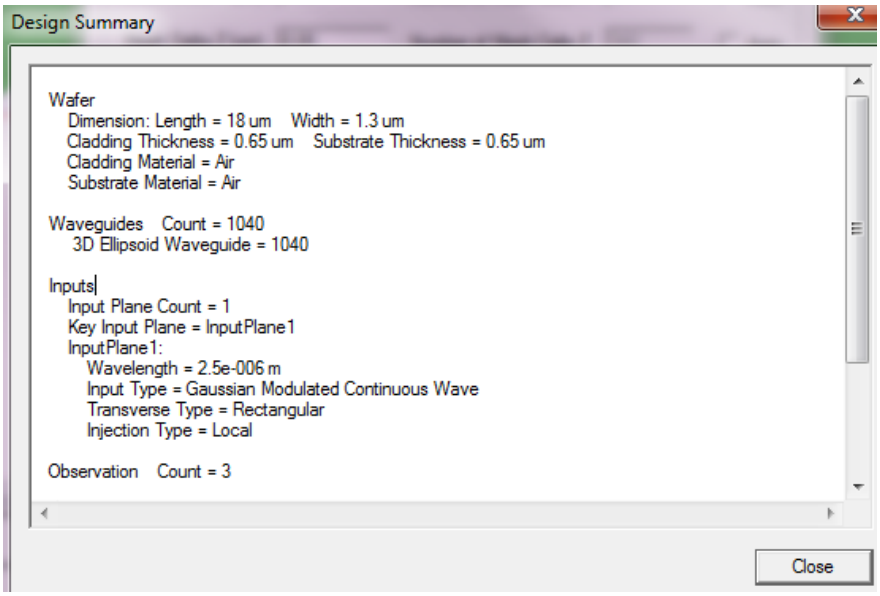

FIGURE A. 4 Design Summary dialog box.

Appendix B: GWL code for LDW system writing

The operation of the Photonic Professional system is controlled by the software Nanowrite. The software interface is shown in Fig. (B.1).

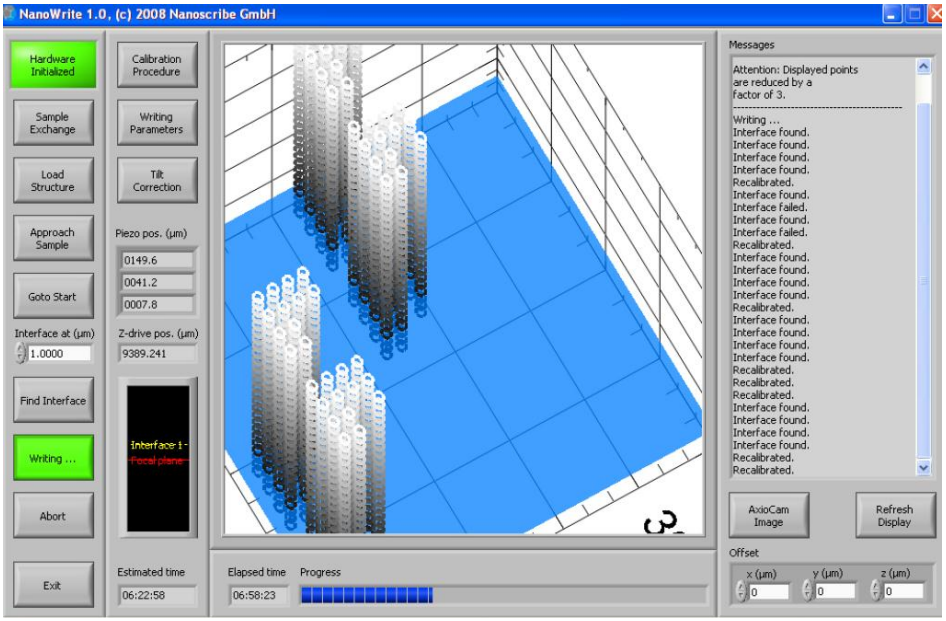

FIGURE B. 1 the graphical user interface of the Nanowrite software.

The most writing parameters are controlled by GWL code as shown below. Each line of the GWL script is used to execute the specific operation like setting up operation mode, line mode, switching on or off the connection points functions et al.

PerfectShapeOff

OperationMode 1

ConnectPointsOn

LineStartMode 1

DwellTime 150

LineNumber 1

PointDistance 20

UpdateRate 1500

PowerScaling 0.3

% use defocus

DefocusFactor 0.62

Xoffset 0

Yoffset 0

Zoffset 0

LaserPower 16

FindInterfaceAt 1

%%%%%%%%%%%%%%%%%%%%

% lattice constant is 2

% radius is 1

% x:10 y: 10 z: 2

1.00000020000000 0 2.40000000000000

1.15643470000000 0.0123117000000000 2.37000000000000

1.30901720000000 0.0489435000000000 2.34000000000000

1.45399070000000 0.108993600000000 2.31000000000000

1.58778540000000 0.190983100000000 2.28000000000000

1.70710690000000 0.292893400000000 2.25000000000000

1.80901710000000 0.412214900000000 2.22000000000000

1.89100660000000 0.546009700000000 2.19000000000000

……

References

1. OptiFDTD Technical Background and tutorials, version 7.0, Optiwave, Inc.

2. Nanoscribe Photonic Professional user manual, version 1.4, Nanoscribe GmbH.